 

*Award Accounts*

**The Chemical Society of Japan Award for 2004**

# Bioinspired Electron-Transfer Systems and Applications

**Shunichi Fukuzumi**

Department of Material and Life Science, Graduate School of Engineering, Osaka University, SORST, Japan Science and Technology Agency, Suita, Osaka 565-0871

Received August 1, 2005; E-mail: fukuzumi@ap.chem.eng.osaka-u.ac.jp

Bioinspired electron-transfer systems including artificial photosynthesis and respiration are presented herein together with some of their applications. First, multi-step electron-transfer systems composed of electron donor–acceptor ensembles have been developed, mimicking functions of the photosynthetic reaction center. However, a significant amount of energy is lost during the multi-step electron-transfer processes. Then, as an alternative to conventional charge-separation functional molecular models based on multi-step long-range electron transfer within redox cascades, simple donor–acceptor dyads have been developed to attain a long-lived and high energy charge-separated state without significant loss of excitation energy, by fine control of the redox potentials and of the geometry of donor–acceptor dyads that have small reorganization energies of electron transfer. Such simple molecular dyads, capable of fast charge separation but extremely slow charge recombination, have significant advantages with regard to synthetic feasibility, providing a variety of applications including construction of organic solar cells and development of efficient photocatalytic systems for the solar energy conversion. An efficient four-electron reduction of dioxygen to water by one-electron reductants such as ferrocene derivatives as well as by an NADH analog has also been achieved as a respiration model by using a cofacial dicobalt porphyrin that can form the $\mu$-peroxo Co(III)–$O_2$–Co(III) complex. The catalytic mechanism of the four-electron reduction of dioxygen has been clarified based on the detailed kinetic study and the detection of the intermediate.

There has been considerable interest in the photosynthetic reaction center of purple bacteria ever since the three-dimensional X-ray crystal structures of reaction centers of *Rhodobacter* (Rb.) *sphaeroides*[1] and other purple bacteria including *Rhodopseudomonas* (Rh.) *viridis*[2] have been disclosed. The photoinduced electron-transfer processes occur in a membrane-bound protein, which contains a number of cofactors, including four bacteriochlorophylls (BChl). Of these, the central part in Fig. 1 is referred to as the special pair [$(BChl)_2$], while the other two bacteriochlorophylls (BChl) are referred to as "accessory" bacteriochlorophylls. There are also two bacteriopheophytins (BPhe), two ubiquinones ($Q_A$ and $Q_B$), and a non-heme iron atom (not shown in Fig. 1), which together with the special pair are organized in pseudo-$C_2$ symmetry forming two branches (A and B). Light-initiated charge separation occurs between the special pair [$(BChl)_2$] and the neighboring pigments, leading to a radical cation [$(BChl)_2^{\bullet+}$]. Despite the quasi-symmetrical arrangement of the cofactors, the electrons are transported unidirectionally along the A-branch of the reaction center,[4–6] which suggests that the symmetry-breaking specific interactions with the protein are fundamentally important. The electron-transfer process is found to occur very rapidly from the special pair toward the quinones to produce a charge-separated state that endures for seconds with a nearly 100% quantum yield.[7] Ultimately, the product of this cascade is conversion of light into usable chemical energy.[8]

The importance and the complexity of energy-transfer and electron-transfer reactions in photosynthesis have prompted the design and preparation of a variety of donor–acceptor covalently linked ensembles including dyads, triads, a tetrad, and a pentad, which can mimic the energy-transfer and electron-transfer processes.[9–17] The extensive efforts devoted so far to achieve the long lifetime and the high efficiency of charge separation mimicking the natural photosynthesis have often been hampered by synthetic difficulties to make the number of covalent bonds needed to connect each component. In addition, the multi-step electron-transfer processes are accompanied by significant energy loss, because each step should be exothermic to reach the final charge-separated (CS) state. Thus, a specific challenge involves construction of simple donor–acceptor dyads, which can afford long-lived and high energy CS states. This account is intended to focus on new approaches to achieve long-lived and high energy CS states using simple donor–acceptor dyads in addition to a conventional strategy based on multi-step long-range electron transfer. Such simple donor–acceptor dyads, capable of fast charge separation but extremely slow charge recombination without significant loss of excitation energy, are shown to have significant advantages with regard not only to synthetic feasibility but also to the applicability for development of efficient solar energy conver-

Published on the web February 10, 2006; DOI 10.1246/bcsj.79.177

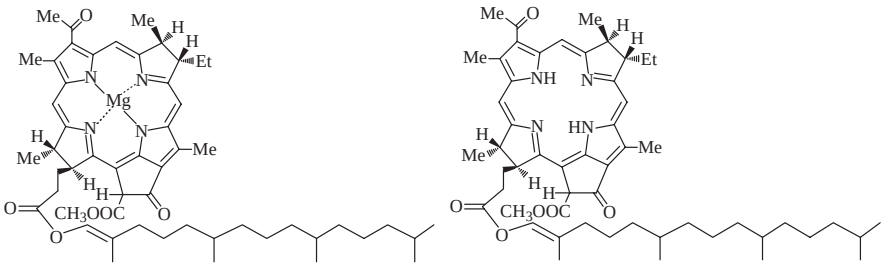

Bacteriochlorophylls (BChl) Bacteriopheophytin (Bphe)

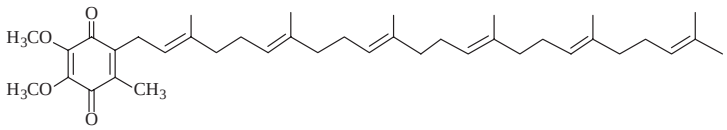

ubiquinone (Q)

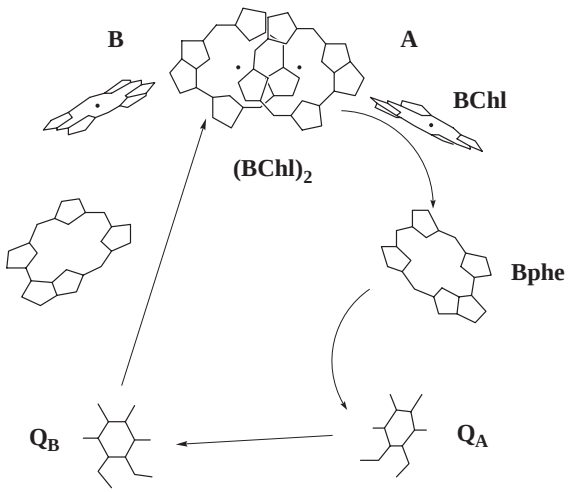


Fig. 1. Cofactors and structure of photosynthetic reaction center of purple bacteria.

sion and photocatalytic systems.

As the reverse process of photosynthesis, in which the four-electron oxidation of water is achieved by using solar energy, the highly exergonic four-electron reduction of oxygen to water is essential to maintain the life of an aerobic organism by the respiration.[18–20] Cytochrome *c* oxidases (C*c*Os) catalyze efficiently the reduction of molecular oxygen to water by the soluble electron carrier, cytochrome *c*.[18–20] The molecular catalytic systems for efficient four-electron reduction of dioxygen are also presented in this account.

## Multi-Step Photoinduced Electron-Transfer Systems, Mimicking the Photosynthetic Reaction Center

According to the Marcus theory of electron transfer,[21] the rate constant of nonadiabatic intramolecular electron transfer ($k_{ET}$) is given by Eq. 1,

$$k_{ET} = \left(\frac{4\pi^3}{h^2\lambda k_B T}\right)^{1/2} V^2 \exp\left[-\frac{(\Delta G_{ET} + \lambda)^2}{4\lambda k_B T}\right], \qquad (1)$$

where $V$ is the electronic coupling matrix element, $h$ is the Planck constant, $T$ is the absolute temperature, $\Delta G_{ET}$ is the free energy change of electron transfer, and $\lambda$ is the reorganization energy of electron transfer. According to Eq. 1, the logarithm of the electron-transfer rate constant ($\log k_{ET}$) is related parabolically to the driving force of electron transfer from electron donors to acceptors ($-\Delta G_{ET}$), and to the reorganization energy ($\lambda$) of electron transfer, that is, the energy required to structurally reorganize the donor, acceptor, and their solvation spheres upon electron transfer. It is now well recognized that the parabolic driving-force dependence of $\log k_{ET}$ (Eq. 1) provides the theoretical basis for understanding electron-transfer processes in photosynthesis.

When the magnitude of the driving force of electron transfer becomes the same as the reorganization energy ($-\Delta G_{ET} \sim \lambda$), the electron-transfer rate reaches a maximum and is basically controlled by the magnitude of electronic coupling ($V$) between the donor and acceptor moiety (Eq. 1). Upon passing this thermodynamic maximum, the highly exothermic region of the parabola ($-\Delta G_{ET} > \lambda$) is entered, in which an additional increase of the driving force results in an actual slow-down of the electron-transfer rate, due to an increasingly poor vibrational overlap of the product and reactant wave functions. This highly exergonic range is generally referred to as the Marcus inverted region.[9–17,22] In such a case, the magnitude of the

reorganization energy is the key parameter to control the electron-transfer process. The smaller the reorganization energy, the faster is the forward photoinduced charge-separation (CS) process, but the charge-recombination (CR) process becomes slower when the driving force for back electron transfer ($-\Delta G_{ET}$) is larger than the reorganization energy ($\lambda$) of electron transfer. Among key parameters that govern electron-transfer reactions ($V$, $\Delta G_{ET}$, and $\lambda$), the reorganization energy ($\lambda$) imposes the most important impact. The primary electron-transfer processes of photosynthesis are, for example, characterized by an extremely small reorganization energy ($\lambda \sim 0.2$ eV), attained by the protein environment. This aspect is essential to achieve the ultrafast charge-separation and retarding the energy-wasting charge-recombination, which is highly exergonic ($-\Delta G = 1.2$ eV).[4–6] Thus, the components of artificial photosynthesis, which are not necessarily natural components in photosynthesis, must have small $\lambda$ values of electron transfer.

The first candidates of such components are porphyrins, which have been involved in a number of important biological electron-transfer systems, including the primary photochemical reactions of chlorophylls in the photosynthetic reaction centers. Porphyrins contain an extensively conjugated two-dimensional $\pi$-system and are thereby suitable for efficient electron transfer, because the uptake or release of electrons results in minimal structural and solvation change upon electron transfer, resulting in a small $\lambda$ value of electron transfer.[23] In addition, rich and extensive absorption features of porphyrinoid systems guarantees increased absorption cross-sections and an efficient use of the solar spectrum.[23] In contrast with the two-dimensional porphyrin $\pi$-system, fullerenes contain an extensively conjugated three-dimensional $\pi$ system.[16] Electron transfer to $C_{60}$ is highly efficient because of the minimal changes of structure and solvation associated with the electron-transfer reduction.[16,24] Thus, a series of porphyrin–fullerene linked molecules have been designed and synthesized to mimic the charge-separation processes in the photosynthetic reaction center, starting from a zinc porphyrin–$C_{60}$ dyad (ZnP–$C_{60}$), a ferrocene–zinc porphyrin–$C_{60}$ triad (Fc–ZnP–$C_{60}$), a zinc porphyrin–free base porphyrin–$C_{60}$ triad, up to a tetrad (Fc–ZnP–$H_2$P–$C_{60}$).[25–30]

The driving-force dependence of the electron-transfer rate constants ($k_{ET}$) of these dyad, triads, and tetrad molecules for CS and CR processes is shown in Fig. 2, where $\log k_{ET}$ is plotted against the driving force ($-\Delta G_{ET}$).[26] The lines in Fig. 2 represent the best fit to Eq. 1 (ZnP–$C_{60}$: $\lambda = 0.66$ eV, $V = 3.9\,cm^{-1}$; Fc–ZnP–$C_{60}$, Fc–$H_2$P–$C_{60}$, and ZnP–$H_2$P–$C_{60}$: $\lambda = 1.09$ eV, $V = 0.019\,cm^{-1}$; Fc–ZnP–$H_2$P–$C_{60}$: $\lambda = 1.32$ eV, $V = 0.00017\,cm^{-1}$).[26] The $\lambda$ value increases, whereas the $V$ value decreases with increasing the edge-to-edge distance in the order of the dyad ($R_{ee} = 11.9$ Å), the triad ($R_{ee} = 30.3$ Å), and the tetrad ($R_{ee} = 48.9$ Å). In the case of the dyad, the CR rate in $ZnP^{\bullet+}$–$C_{60}^{\bullet-}$ in the Marcus inverted region is much slower than the CS rate constants from both the singlet and triplet excited states in the Marcus normal region (Fig. 2). This enables a subsequent electron transfer from Fc to $ZnP^{\bullet+}$ in the triad (Fc–$ZnP^{\bullet+}$–$C_{60}^{\bullet-}$) and from ZnP to $H_2P^{\bullet+}$ in ZnP–$H_2P^{\bullet+}$–$C_{60}^{\bullet-}$ to produce the final CS state, $Fc^+$–ZnP–$C_{60}^{\bullet-}$ and $ZnP^{\bullet+}$–$H_2$P–$C_{60}^{\bullet-}$, in competition with the back electron transfer in the initial CS states. In the case of the tetrad (Fc–ZnP–$H_2$P–$C_{60}$), the multi-step electron-transfer processes afford the final CS state, $Fc^+$–ZnP–$H_2$P–$C_{60}^{\bullet-}$, in which charges are separated at a long distance ($R_{ee} = 48.9$ Å).[26] The lifetime of the resulting CS state at such a long distance in a frozen PhCN has been determined to be as long as 0.38 s.[26] It should be noted that the CS lifetime is temperature independent, since the CR process is at the Marcus top region (Fig. 2). This is the first example to achieve a CS lifetime which is comparable to that observed for the bacterial photosynthetic reaction center. However, such an extremely long CS lifetime could only be determined in frozen media, since in condensed media bimolecular back electron transfer between two $Fc^+$–ZnP–$H_2$P–$C_{60}^{\bullet-}$ is much faster than the unimolecular CR process.[26]

The maximum $k_{ET}$ value ($k_{ETmax}$) of each Marcus plot in Fig. 2 is correlated with the edge-to-edge distance ($R_{ee}$), separating the radical ions, according to Eq. 2,[26]

$$\ln k_{ETmax} = \ln\left(\frac{2\pi^{3/2}V_0^2}{h(\lambda k_B)^{1/2}}\right) - \beta R_{ee}, \quad (2)$$

where $V_0$ refers to the maximal electronic coupling element, while $\beta$ is the decay coefficient factor (damping factor), which depends primarily on the nature of the bridging molecule. From the linear plot of $\ln k_{ETmax}$ vs $R_{ee}$ the $\beta$ value is obtained as $0.60\,Å^{-1}$.[26] This $\beta$ value is located within the boundaries of nonadiabatic electron-transfer reactions for saturated hydrocarbon bridges (0.8–1.0 $Å^{-1}$) and unsaturated phenylene bridges ($0.4\,Å^{-1}$).[31]

The best molecule mimicking multi-step electron-transfer processes in the photosynthetic reaction center so far reported is a ferrocene–*meso*,*meso*-linked porphyrin trimer–fullerene pentad (Fc–$(ZnP)_3$–$C_{60}$ in Scheme 1), where the $C_{60}$ and the ferrocene (Fc) are tethered at both the ends of $(ZnP)_3$ ($R_{ee} = 46.9$ Å).[32] The lifetime of the final CS state (0.53 s at 163 K) has been attained without lowering the CS efficiency ($\Phi = 0.83$).[32]

## Simple Donor–Acceptor Dyads with Much Longer CS Lifetimes than Natural Photosynthetic Reaction Centers

Multi-step electron-transfer processes have been utilized to attain a long distance charge separation, mimicking the natural photosynthetic reaction center (vide supra). However, a significant amount of energy is lost during the multi-step electron-transfer processes to reach the final CS state.[4–6] In the photosynthesis, two-step photoexcitation, a so-called "Z-scheme," is thereby required to recover the energy loss via the multi-step electron-transfer processes and to gain the strong oxidizing power to oxidize water as well as the high reducing power to reduce $NAD^+$ coenzyme.[8,33] The design and synthesis of molecular machinery mimicking such an elaborated "Z-scheme" in nature seems far beyond our capability; even if it could be done, the synthetic cost would certainly preclude any type of practical application. Thus, it is highly desired to design simple molecular electron donor–acceptor dyads which are capable of fast charge separation but retain slow charge recombination. Theoretically, it is possible to obtain such an electron donor–acceptor dyad, because the CS lifetime increases with increasing the driving force of electron transfer in the Marcus inverted region (vide supra). However, the driving force of

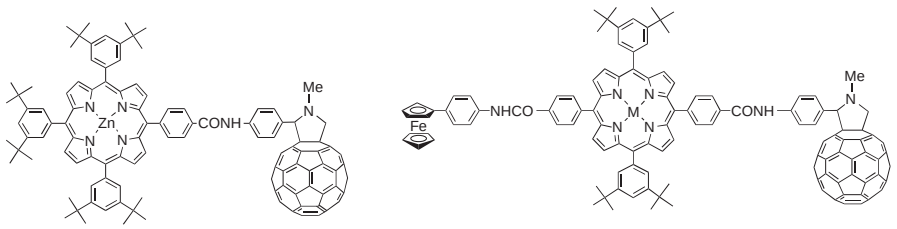


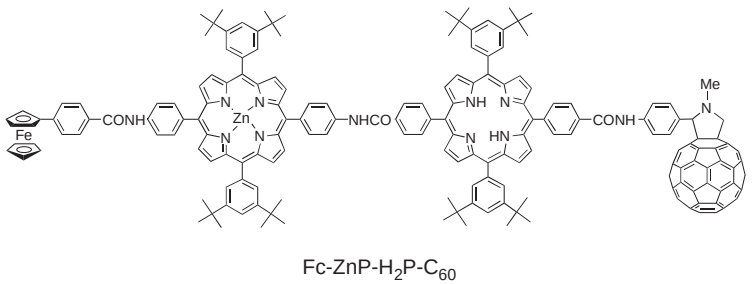


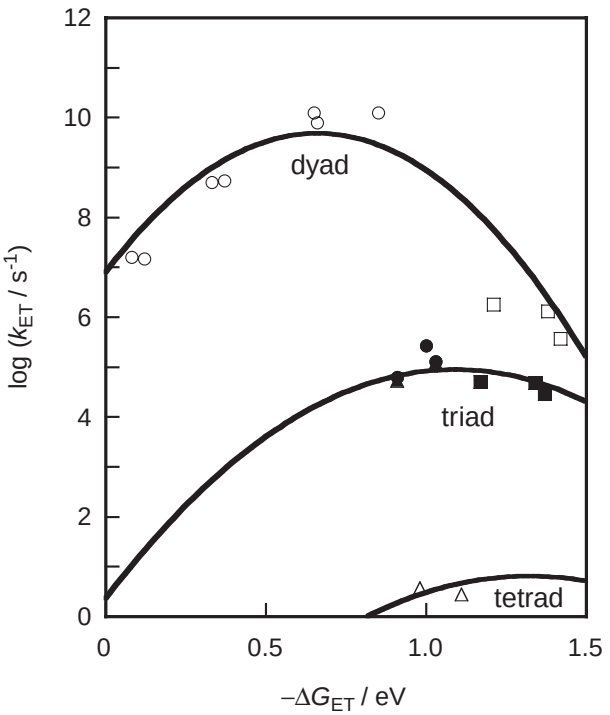


Fig. 2. Driving-force ($-\Delta G_{ET}$) dependence of intramolecular electron-transfer rate constants ($k_{ET}$) in ZnP–$C_{60}$ (CS: white circles; CR: white squares), Fc–ZnP–$C_{60}$ (black circles), Fc–$H_2$P–$C_{60}$ (black triangles), ZnP–$H_2$P–$C_{60}$ (black squares), and Fc–ZnP–$H_2$P–$C_{60}$ (white triangles).

electron transfer should be lower than the triplet excited state of one of the components of donor–acceptor dyads. Otherwise, the CS state would decay rapidly to the triplet excited state in the Marcus normal region rather than to the ground state in the Marcus inverted region.[27]

A number of simple donor–acceptor dyads have been designed and synthesized to attain a long-lived CS state, where the donor and acceptor molecules are linked with a short spacer to minimize the solvent reorganization energy.[34–39] Efficient photoinduced electron transfer occurs in a zinc imidazoporphyrin–$C_{60}$ dyad (ZnImP–$C_{60}$) with a short linkage to form the CS state (ZnImP$^{\bullet+}$–$C_{60}^{\bullet-}$) with the rate constant of $1.4 \times 10^{10}\,s^{-1}$ (Scheme 2).[34] The CS state (1.34 eV) is lower in energy than both the triplet excited states of $C_{60}$ (1.50 eV) and ZnImP (1.36 eV).[34] The CS state, produced upon photoexcitation of ZnImP–$C_{60}$, is detected by the transient absorption spectrum, which has the absorption bands at 700 and 1040 nm due to ZnImP$^{\bullet+}$ and $C_{60}^{\bullet-}$, respectively.[34] The CS state decays by back electron transfer to the ground state, obeying first-order kinetics with the rate constant of $3.9 \times 10^{3}\,s^{-1}$

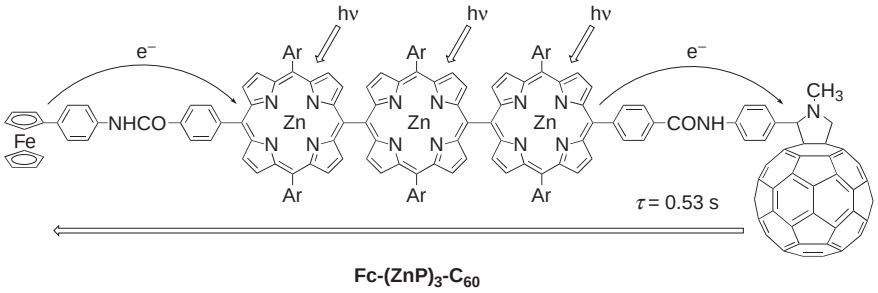


Scheme 1. Multi-step photoinduced electron transfer in a ferrocene–*meso*,*meso*-linked porphyrin trimer–fullerene pentad (Fc–$(ZnP)_3$–$C_{60}$); Ar = 3,5-$Bu^t{}_2C_6H_3$.[32]

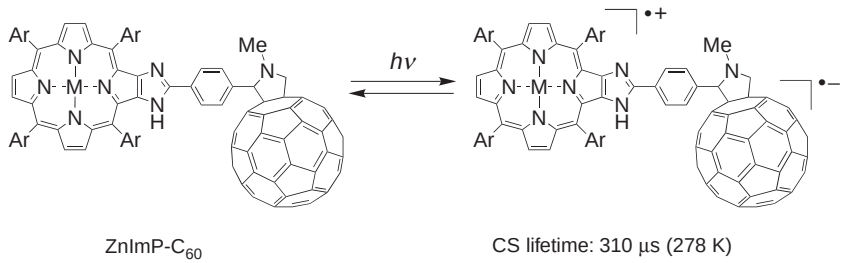


Scheme 2. Formation of a long-lived CS state of a zinc imidazoporphyrin–$C_{60}$ dyad (ZnImP–$C_{60}$) with a short linkage (Ar = 3,5-$Bu^t{}_2C_6H_3$).[34]

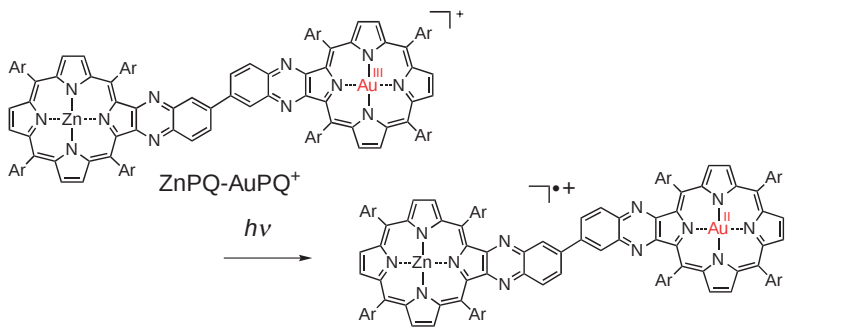


Scheme 3. Formation of a long-lived CS state of ZnPQ–$AuPQ^+$ in non-polar solvents (Ar = 3,5-$Bu^t{}_2C_6H_3$).[35]

(the lifetime is 260 μs) at 298 K.[34] At 278 K the lifetime of the CS state was determined as 310 μs, which is much longer than those of conventional donor–acceptor dyads with longer spacers.[9–17]

An electron donor–acceptor dyad linked with a short spacer containing Au(III) and Zn(II) porphyrins (ZnPQ–$AuPQ^+$ in Scheme 3) also affords a long-lived electron-transfer state with the lifetime of 10 μs in a nonpolar solvent such as cyclohexane.[35] The introduction of quinoxaline to the gold porphyrin results in a lowering of the electron-transfer state energy. In contrast to the case of neutral donor–acceptor dyads, the energy of the electron-transfer state ($ZnPQ^{\bullet+}$–$Au^{II}PQ$) becomes smaller in a less polar solvent, which is lower than the energies of the triplet excited states of ZnPQ (1.32 eV) and $AuPQ^+$ (1.64 eV).[35] Photoinduced electron transfer occurs from the singlet excited state of the ZnPQ ($^1ZnPQ^*$) to the metal center of the $AuPQ^+$ moiety to produce $ZnPQ^{\bullet+}$–$Au^{II}PQ$. The observed long lifetime of $ZnPQ^{\bullet+}$–$Au^{II}PQ$ results from a small reorganization energy for the *metal-centered* electron transfer of $AuPQ^+$ in nonpolar solvents due to the small change in solvation upon the electron transfer as compared with that in polar solvents. In a polar solvent such as benzonitrile (PhCN), no CS state was observed, but instead only the triplet–triplet absorption due to $^3ZnPQ^*$–$AuPQ^+$ was observed.[35] The absence of an observable CS state in PhCN is ascribed to the much slower photoinduced electron transfer due to the large reorganization energy as compared with that in nonpolar solvents allowing an efficient intersystem crossing process in the ZnPQ–$AuPQ^+$ dyad to produce the triplet excited state $^3ZnPQ^*$–$AuPQ^+$.

A closely linked zinc chlorin–fullerene dyad (ZnCh–$C_{60}$ in Fig. 3) affords the longer CS lifetime as compared with other zinc chlorin–fullerene dyads with the longer spacers.[36–40] A deoxygenated PhCN solution containing ZnCh–$C_{60}$ gives rise upon a 388 nm laser pulse to a transient absorption maximum at 460 nm due to the singlet excited state of ZnCh.[36] The decay rate constant was determined as $1.0 \times 10^{11}$ $s^{-1}$, which agrees with the value determined from the fluorescence

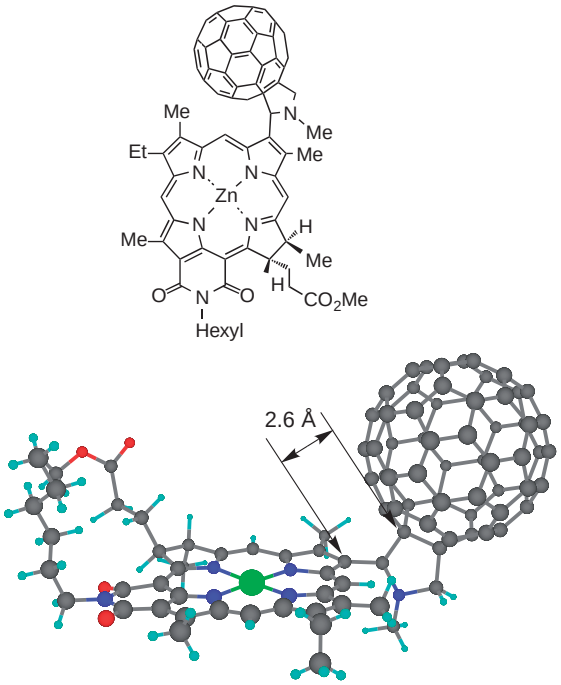


Fig. 3. Structure of a closely linked ZnCh–$C_{60}$ dyad.

lifetime measurements.[36] The decay of absorbance at 460 nm due to $^1$ZnCh* is accompanied by an increase in absorbance at 590 nm due to ZnCh$^{\bullet+}$.[36] This indicates that electron transfer from $^1$ZnCh* to $C_{60}$ occurs rapidly to form the CS state, ZnCh$^{\bullet+}$–$C_{60}^{\bullet-}$. The CS state decays via back electron transfer to the ground state rather than to the triplet excited state, since the CS state is lower in energy (1.26 eV) than both the triplet excited state of $C_{60}$ (1.50 eV) and ZnCh (1.36–1.45 eV).[36] The lifetime of the CS state is determined as 230 μs at 298 K. The large temperature dependence of the CS lifetime is observed and the lifetime of the CS state at 123 K becomes as long as 120 s.[36]

Covalently and non-covalently linked porphyrin–quinone dyads constitute one of the most extensively investigated photosynthetic models, in which the fast photoinduced electron transfer from the porphyrin singlet excited state to the quinone occurs to produce the CS state, mimicking well the photosynthetic electron transfer.[41–43] Unfortunately, the CR rates of the CS state of porphyrin–quinone dyads are also fast and the CS lifetimes are mostly on the order of picoseconds or subnanoseconds in solution.[41–43] In general, a three-dimensional $C_{60}$ is superior to a 2-dimentional quinone in terms of the smaller reorganization of electron transfer of $C_{60}$ as compared with quinone (vide supra) to attain the long-lived CS state.[16,44] When the geometry between a porphyrin ring and quinone is optimized by using hydrogen bonds which can also control the redox potentials of quinones, however, a surprisingly long lifetime up to a microsecond has been attained.[45] In a series of ZnP–*n*–Q ($n = 3$, 6, and 10) in Scheme 4, the hydrogen bond between two amide groups provides a structural scaffold to assemble the donor (ZnP) and the acceptor (Q) moiety, allowing one to attain the long-lived CS state.[45]

As described above, the closely linked donor–acceptor dyads afford long-lived CS states. As long as porphyrins and $C_{60}$

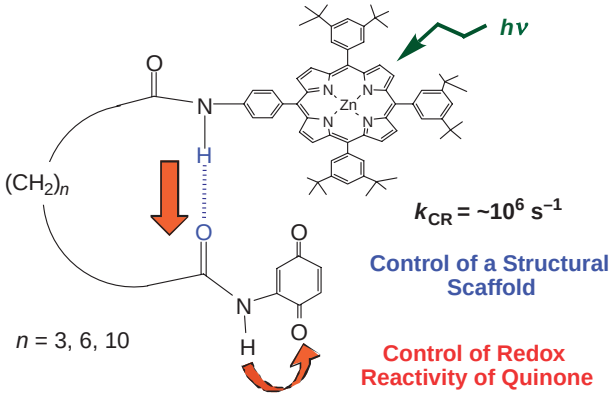


Scheme 4. Zinc porphyrin–quinone linked dyads (ZnP–*n*–Q; $n = 3$, 6, and 10) with hydrogen bonds.[45]

are used as components of donor–acceptor dyads, however, the low lying triplet energies of porphyrins and $C_{60}$ have precluded attempts to attain the long-lived CS states with a higher energy than the triplet energies.[27] In such a case, it is highly desired to find a chromophore which has a high triplet energy and a small $\lambda$ value of electron transfer. Acridinium ion is the best candidate for such a purpose, since the $\lambda$ value for the electron self-exchange between the acridinium ion and the corresponding one-electron reduced radical is the smallest (0.3 eV) among the redox active organic compounds.[46] Another important property of acridinium ion is a high triplet excited energy.[47,48] Thus, an electron-donor moiety (mesityl group) is directly connected at the 9-position of the acridinium ion to yield 9-mesityl-10-methylacridinium ion (Acr$^+$–Mes),[49] in which the solvent reorganization of electron transfer is minimized because of the short linkage between the donor and acceptor moieties. The X-ray crystal structure of Acr$^+$–Mes is shown in Fig. 4a.[49] The dihedral angle made by aromatic ring planes is perpendicular, and thus there is no $\pi$ conjugation between the donor and acceptor moieties. Indeed, the absorption and fluorescence spectra of Acr$^+$–Mes are superpositions of the spectra of each component, i.e., mesitylene and 10-methylacridinium ion. The HOMO and LUMO orbitals of Acr$^+$–Mes calculated by a DFT method with Gaussian 98 (B3LYP/6-31G* basis set) are localized on mesitylene and acridinium moieties (Figs. 4b and 4c), respectively. The energy of the electron-transfer state (Acr$^\bullet$–Mes$^{\bullet+}$) is determined by the redox potentials of each component of Acr$^+$–Mes as 2.37 eV.[49]

Photoirradiation of a deaerated PhCN solution of Acr$^+$–Mes by a nanosecond laser light flash at 430 nm results in formation of Acr$^\bullet$–Mes$^{\bullet+}$ with a quantum yield close to unity (98%) via photoinduced electron transfer from the mesitylene moiety to the singlet excited state of the acridinium ion moiety ($^1$Acr$^{+*}$–Mes). The intramolecular back electron transfer from the Acr$^\bullet$ moiety to the Mes$^{\bullet+}$ moiety in Acr$^\bullet$–Mes$^{\bullet+}$ was too slow to compete with the intermolecular back electron-transfer reaction, when the decay time profile of Acr$^\bullet$–Mes$^{\bullet+}$ obeyed second-order kinetics (NOT first-order kinetics).[49] This is the same as the case of Fc$^+$–ZnP–$H_2$P–$C_{60}^{\bullet-}$, in which bimolecular back electron transfer predominates due to the slow intramolecular back electron transfer (vide supra).[26] In contrast, the decay of Acr$^\bullet$–Mes$^{\bullet+}$ obeys first-order kinetics in PhCN at high temperatures. This indicates that the rate of the intra-

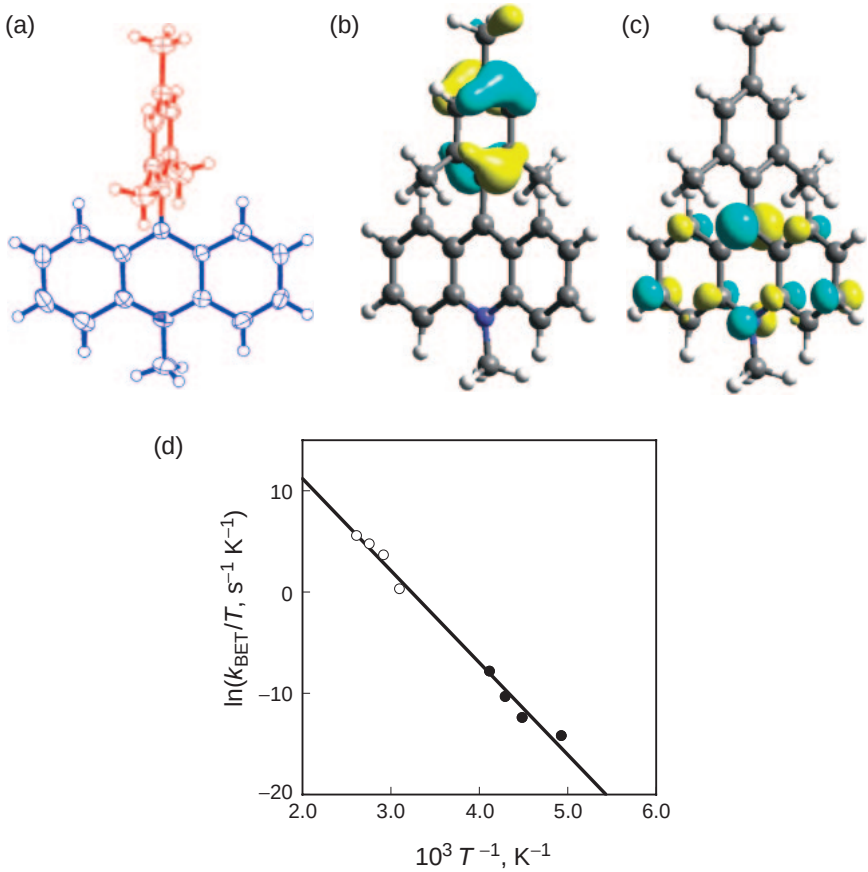


Fig. 4. (a) X-ray crystal structure of $Acr^+$–Mes. (b) HOMO and, (c) LUMO orbitals calculated by a DFT method with Gaussian 98 (B3LYP/6-31G* basis set). (d) Plot of $k_{BET}/T$ vs $T^{-1}$.

molecular back electron transfer of $Acr^{\bullet}$–$Mes^{\bullet+}$ becomes much faster than the rate of the intermolecular back electron transfer at higher temperatures because the activation energy of the former is higher than that of the latter. A large temperature dependence of the rate constant of intramolecular back electron transfer ($k_{BET}$) in Fig. 4d agrees with the Marcus equation in the deeply inverted region (Eq. 1). The lifetime of the electron-transfer state becomes longer with decreasing temperature, to approach a virtually infinite value at 77 K. Such a remarkable result has sparked a flurry of work by others in the field of artificial photosynthesis.[50]

Benniston et al. have recently claimed that the triplet excited state of the acridinium ion moiety ($^3Acr^{+*}$–Mes) might be formed rather than the electron-transfer state ($Acr^{\bullet}$–$Mes^{\bullet+}$) and that the energy of $^3Acr^{+*}$–Mes is lower than that of $Acr^{\bullet}$–$Mes^{\bullet+}$.[51] They reported that the triplet excitation energy of $Acr^+$–Mes was 1.96 eV based on the phosphorescence spectrum.[51] If this value were correct, the one-electron oxidation potential ($E_{ox}$) of $^3Acr^{+*}$–Mes would be −0.08 V vs SCE, which is determined from the one-electron oxidation potential of the Mes moiety (1.88 V)[49] and the triplet excitation energy (1.96 V). In such a case, electron transfer from the triplet excited state of $Acr^+$–Mes to *N*,*N*-dihexylnaphthalenediimide (NIm: $E_{red} = -0.46$ V vs SCE) would be energetically impossible judging from the positive free energy change of electron transfer (0.38 eV). However, the addition of NIm ($1.0 \times 10^{-3}$ M) to a PhCN solution of $Acr^+$–Mes and the laser photoexcitation results in the formation of $NIm^{\bullet-}$ as detected by the well-known absorption bands at 480 and 720 nm,[52,53] accompanied by the decay of transient absorption at 510 nm due to the $Acr^{\bullet}$ moiety of the ET state as shown in Fig. 5a.[54] Similarly, the addition of aniline ($3.0 \times 10^{-5}$ mol dm$^{-3}$) to a PhCN solution of $Acr^+$–Mes results in formation of aniline radical cation ($\lambda_{max} = 430$ nm),[55] accompanied by decay of the $Mes^{\bullet+}$ moiety at 500 nm as shown in Fig. 5b.[54] The formation rate constant of aniline radical cation is determined as $5.6 \times 10^9$ mol$^{-1}$ dm$^3$ s$^{-1}$, which is close to the diffusion rate constant in PhCN.

Thus, the photogenerated state of $Acr^+$–Mes has both the reducing and the oxidizing ability: to reduce NIm and to oxidize aniline, respectively. Only the electron-transfer state ($Acr^{\bullet}$–$Mes^{\bullet+}$) has such a dual ability. However, this conclusion is contradictory to the triplet energy (1.96 eV), which was reported to be lower in energy than the electron-transfer state by Benniston et al.[51] This contradiction comes from an impurity involved in the preparation of $Acr^+$–Mes by Benniston et al. who synthesized the compound via methylation of the corresponding acridine.[51] The yield of acridinium ion is about 50–70% after reflux at high temperature for a few days.[51] In such a case, acridine may remain as an impurity even after purification of acridinium ion by recrystallization. In our case, $Acr^+$–Mes was prepared by the Grignard reaction of 10-methyl-9(10*H*)-acridone with 2-mesitylmagnesium bromide without involving methylation.[49] Our purified $Acr^+$–Mes has

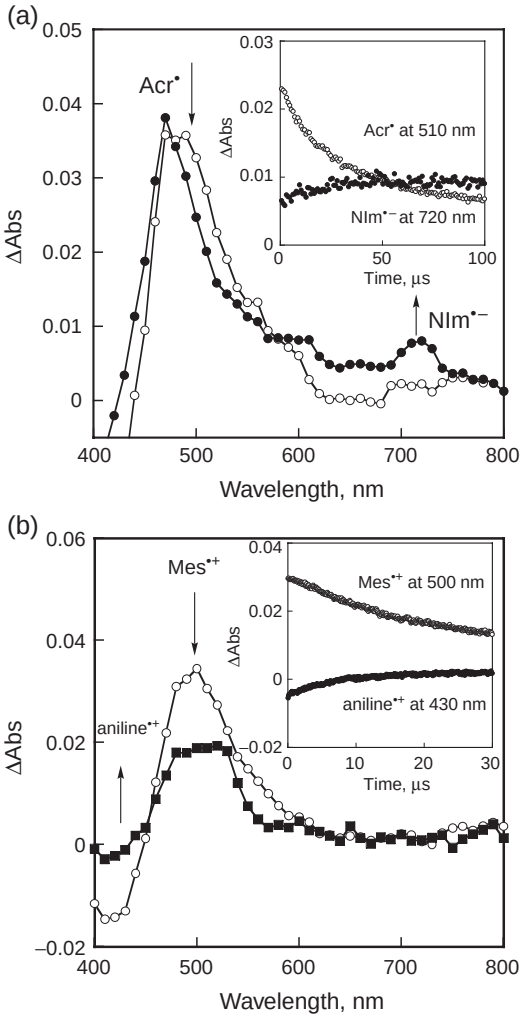


Fig. 5. Transient absorption spectra of $Acr^+$–Mes ($5.0 \times 10^{-5}$ mol dm$^{-3}$) in deaerated MeCN at 298 K taken at 2 and 20 μs after laser excitation at 430 nm in the presence of (a) *N*,*N*-dihexylnaphthalenediimide ($1.0 \times 10^{-3}$ mol dm$^{-3}$) or (b) aniline ($3.0 \times 10^{-5}$ mol dm$^{-3}$). Inset: time profiles of the absorbance decay at 510 and the rise at 720 nm and (b) the decay at 500 nm and the rise at 430 nm.

thereby afforded no phosphorescence spectrum in both deaerated glassy 2-MeTHF and ethanol at 77 K. It is well known that acridine derivatives exhibit phosphorescence at 15650–15850 cm$^{-1}$.[56] It was confirmed that the phosphorescence maximum of 9-phenylacridine in glassy 2-MeTHF at 77 K afforded a quite similar spectrum to that reported by Benniston et al.[51] Thus, the reported low triplet energy of $Acr^+$–Mes, which contradicts to our results on the long-lived electron-transfer state, may result from the acridine impurity contained in the $Acr^+$–Mes used by Benniston et al.

Benniston et al. also reported that photoirradiation of a PhCN solution of $Acr^+$–Mes results in formation of the acridinyl radical ($Acr^•$–Mes).[51] They implied that this stable radical species could be mistaken as a long-lived electron-transfer state.[51] When PhCN is purified, however, no change in the absorption spectrum is observed (Fig. 6a).[46,54] The formation of $Acr^•$–Mes results from electron transfer from an donor impurity contained in unpurified PhCN (e.g., aniline) to the $Mes^{•+}$ moiety of $Acr^•$–$Mes^{•+}$ as indicated in Fig. 5b. Even an extremely small amount ($5.0 \times 10^{-5}$ mol dm$^{-3}$) of aniline is enough to react with $Acr^•$–$Mes^{•+}$ to produce $Acr^•$–Mes, which is stable due to the bulky Mes substituent, because the lifetime of $Acr^•$–$Mes^{•+}$ is long enough to react with such a small concentration of an electron donor. It should be noted that no net photochemical reaction occurs without a donor impurity because the long-lived $Acr^•$–$Mes^{•+}$ decays via bimolecular back electron transfer to the ground state.[46,54] Thus, misleading effects of impurities indeed result from the long-lived electron-transfer state which has both oxidizing and reducing ability.

In contrast to the photoirradiation of a purified PhCN solution of $Acr^+$–Mes at 298 K, which results in no change in the absorption spectrum (Fig. 6a), when the photoirradiation of the same solution was performed at low temperatures (213–243 K) with a 1000 W high-pressure mercury lamp through the UV light cutting filter (>390 nm) and the sample was cooled to 77 K, the color of the frozen sample at 77 K was clearly changed from green to brownish as shown in the inset of Fig. 6b. When a glassy 2-methyltetrahydrofuran (2-MeTHF) is employed for the photoirradiation of $Acr^+$–Mes at low temperature, the resulting glassy solution measured at 77 K affords the absorption spectrum due to the electron-transfer state, which consists of the absorption bands of the $Acr^•$ moiety (500 nm) and the $Mes^{•+}$ moiety (470 nm), as shown in Fig. 6b. No decay of the absorption due to the electron-transfer state in Fig. 6b was observed until liquid nitrogen runs out.[54]

## Effects of Metal Ions on Photoinduced Electron Transfer

Long-lived CS states have been successively achieved by minimizing the reorganization energy of electron transfer in the Marcus inverted region (vide supra). In principle, the totally opposite approach to attain long-lived CS states is possible, that is the use of a component with a large reorganization energy, which results in slow back electron transfer in the Marcus normal region ($-\Delta G_{ET} < \lambda$). In such a case, however, the rate of forward electron transfer with a much smaller driving force becomes much smaller than the back electron-transfer rate, and thus the use of a component with a large organization energy has never been employed to design the artificial photosynthetic reaction center. If one can design a system in which the forward electron transfer has a small reorganization energy whereas the reorganization energy of the back electron transfer becomes much larger than that of the forward electron transfer in the Marcus normal region, long-lived charge-separated states would be attained efficiently. In the Marcus normal region, the smaller the driving force, the smaller is the electron-transfer rate (Eq. 1). Thus, a decrease in the driving force of back electron transfer is essential to attain the long-lived charge-separated states in the Marcus normal region. The driving force of electron transfer has been shown to be finely controlled by complexation of radical anions, produced in the electron transfer, with metal ions which act as Lewis acids, in a variety of intermolecular and intramolecular electron-transfer systems.[57–61] Quantitative measurements to determine the Lewis acidity of a variety of metal ions have been well established in relation with the promoting effects of metal ions on the electron-transfer reactions.[62]

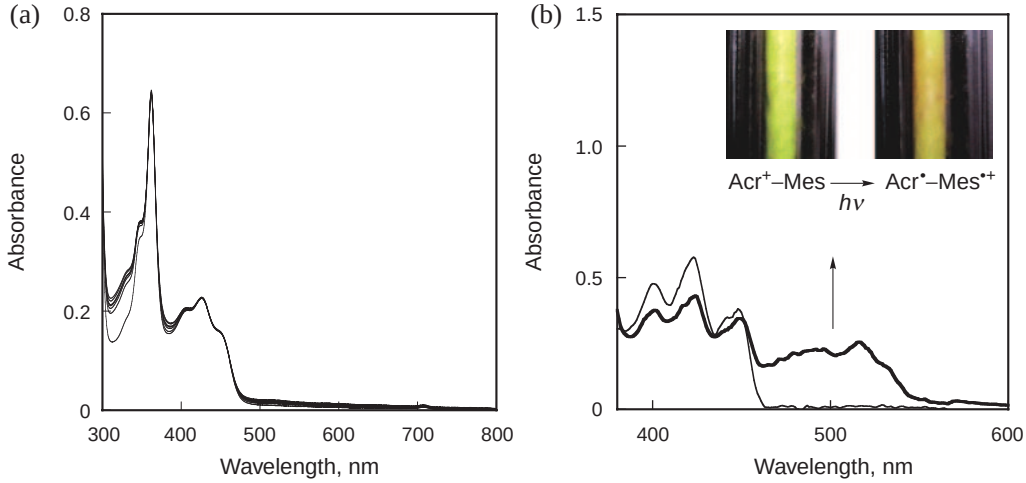


Fig. 6. (a) UV–vis spectral change in the steady-state photolysis of a deaerated PhCN solution of $Acr^+$–Mes ($3.3 \times 10^{-5}$ mol $dm^{-3}$). Spectra were recorded at 90 s interval. (b) UV–vis absorption spectra obtained by photoirradiation with high-pressure mercury lamp of deaerated 2-MeTHF glasses of $Acr^+$–Mes at 77 K. Inset: picture images of frozen PhCN solutions of $Acr^+$–Mes before and after photoirradiation at low temperatures and taken at 77 K.

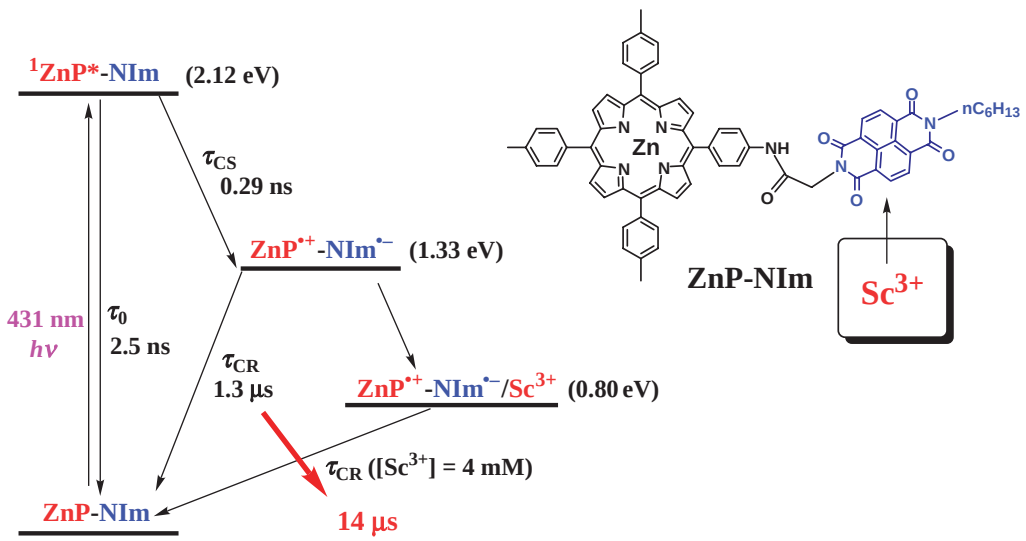


Scheme 5. Energy diagram and photodynamics of a zinc porphyrin–naphthalenediimide (ZnP–NIm) dyad in the absence and presence of a metal ion.[63]

Significant effects of metal ions on photoinduced electron transfer in porphyrin-containing donor–acceptor ensembles, a zinc porphyrin–naphthalenediimide (ZnP–NIm) dyad, have been reported as shown in Scheme 5.[63] The photoexcitation of ZnP–NIm results in formation of the singlet excited state ($^1$ZnP*–NIm: 2.12 eV) in which electron transfer from $^1$ZnP* to NIm occurs to give the CS state ($ZnP^{\bullet+}$–$NIm^{\bullet-}$) with the rate constant, $k_{CS} = 3.4 \times 10^9\ s^{-1}$, in competition with the decay to the ground state with $k_0 = 4.0 \times 10^8\ s^{-1}$. The back electron transfer from $NIm^{\bullet-}$ to $ZnP^{\bullet+}$ (CR) occurs with $k_{CR} = 7.7 \times 10^5\ s^{-1}$. In the presence of metal ions ($M^{n+}$), the CS process takes place mainly from $^1$ZnP*–NIm rather than $^1$ZnP*–NIm/$M^{n+}$ complex due to very weak binding of $M^{n+}$ with the neutral species of NIm. In such a case, the $k_{CS}$ values in the presence of $M^{n+}$ are determined by the $-\Delta G_{CS}$ value in the absence of $M^{n+}$ rather than the $-\Delta G_{CS}$ values in the presence of $M^{n+}$, although the $-\Delta G_{CS}$ values increase with increasing [$M^{n+}$]. In contrast, the $k'_{CR}$ values in the presence of $M^{n+}$ are determined by the $-\Delta G_{CR}$ values in the presence of $M^{n+}$, since the CR process occurs mainly from the $ZnP^{\bullet+}$–$NIm^{\bullet-}/M^{n+}$ complex rather than from $ZnP^{\bullet+}$–$NIm^{\bullet-}$. The back electron transfer from $NIm^{\bullet-}$ to $ZnP^{\bullet+}$ (CR) in the presence of $1.0 \times 10^{-3}$ M $Sc^{3+}$ occurs with $k'_{CR} = 6.9 \times 10^4\ s^{-1}$. The decrease in the CR driving force together with an increase in the $\lambda$ value in the presence of $M^{n+}$ results in elongation of the CS lifetime.[63] The effect of metal ion is the largest for $Sc^{3+}$ ion, which is the strongest Lewis acid among metal ions.[62]

A remarkable seven million times elongation of the CS lifetime is attained by complex formation of yttrium triflate [$Y(OTf)_3$] with the CS state in photoinduced electron transfer of a ferrocene–anthraquinone dyad (Fc–AQ) involving a rigid amide spacer (Scheme 6).[64] Photoexcitation of the AQ moiety

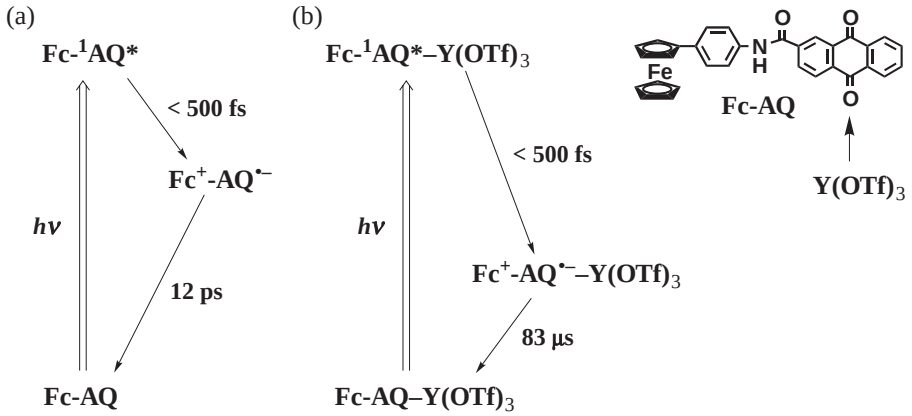


Scheme 6. Photodynamics of a ferrocene–anthraquinone dyad (Fc–AQ) (a) in the absence and (b) in the presence of $Y(OTf)_3$.[65]

in Fc–AQ in deaerated PhCN with femtosecond (150 fs width) laser light results in the appearance of the absorption bands around 420 and 600 nm at 500 fs.[64] The absorption bands around 420 and 600 nm are assigned to $AQ^{\bullet-}$ by comparison with the absorption spectrum of $AQ^{\bullet-}$ produced by the chemical reduction of AQ with naphthalene radical anion.[64] The decay process obeys first-order kinetics with the lifetime of 12 ps.[64] This indicates that electron transfer from Fc to the singlet excited state of AQ occurs efficiently to produce the CS state ($Fc^+$–$AQ^{\bullet-}$) within 500 fs and decays via back electron transfer to the ground state with a lifetime of 12 ps (Scheme 6a).

In the presence of $Y(OTf)_3$ ($1.0 \times 10^{-2}$ M) as well, photoexcitation of the Fc–AQ system using a femtosecond laser results in efficient electron transfer from Fc to AQ within 500 fs.[64] However, the transient absorption band observed at 700 nm in the presence of $Y(OTf)_3$ is significantly red-shifted as compared with that observed at 600 nm in the absence of $Y(OTf)_3$.[64] Such a red shift has been reported for the complex formation of semiquinone radical anions with metal ions.[61] The decays of absorbance at 420 and 700 nm due to the $Fc^+$–$AQ^{\bullet-}$–$Y(OTf)_3$ complex obey first-order kinetics to afford the identical CS lifetime that is determined as 83 μs.[64] The CS lifetime is seven million times longer than the lifetime in the absence of $Y(OTf)_3$ (12 ps). The strong binding of $Y(OTf)_3$ with $AQ^{\bullet-}$ results in a substantial deceleration of the back electron transfer from $AQ^{\bullet-}$ to $Fc^+$, leading to a remarkable elongation of the CS lifetime, whereas the forward photoinduced electron transfer in both the absence and the presence of $Y(OTf)_3$ takes place within 500 fs (Scheme 6b).[64]

Such a remarkable effect of $Y^{3+}$ on controlling the electron-transfer processes of quinones has enabled us to develop a highly $Y^{3+}$-selective fluorescence sensor using a zinc porphyrin–CONH–quinone dyad (ZnP–CONH–Q), as shown in Fig. 7.[65] ZnP–NHCO–Q linked dyad and the reference compound (ZnP–CONH–ref) are also employed for comparison. The fluorescence intensities of ZnP–CONH–Q and ZnP–NHCO–Q are significantly quenched as compared with that of ZnP–CONH–ref in deaerated PhCN via photoinduced electron transfer from the singlet excited state of the ZnP moiety to the Q moiety.[65]

Addition of a small concentration of $Y(OTf)_3$ ($10^{-6}$ M–$10^{-3}$ M) to a deaerated PhCN solution of ZnP–CONH–Q results in a remarkable enhancement of the ZnP fluorescence intensity. From the fluorescence titration of $Y^{3+}$ in ZnP–CONH–Q, the binding constant ($K$) between $Y^{3+}$ and ZnP–CONH–Q is estimated as 3900 $M^{-1}$ in deaerated PhCN.[65] The fluorescence intensities of ZnP–CONH–Q (3 μM) and ZnP–NHCO–Q (3 μM) in the presence of 400 μM concentration of various metal ions in reference to those in the absence of metal ion are determined in deaerated PhCN, as shown in Fig. 7.[65] A remarkable enhancement of the fluorescence intensity is observed exclusively in the case of ZnP–CONH–Q in the presence of $Y^{3+}$, whereas ZnP–NHCO–Q exhibits only moderate enhancement of the fluorescence intensity in the presence of metal ions. Such a significant difference in the fluorescent intensity between ZnP–CONH–Q and ZnP–NHCO–Q in the presence of $Y^{3+}$ indicates that the binding sites of ZnP–CONH–Q to $Y^{3+}$ are more suitable than those of ZnP–NHCO–Q. This is supported by the optimized structure of the Ph–CONH–Q/$Y^{3+}$ complex that is evaluated by ADF calculation with II (large) basis set, as shown in the inset of Fig. 7; the result demonstrates the strong binding of $Y^{3+}$ with two carbonyl oxygens of ZnP–CONH–Q.[65] The $Y^{3+}$-selective enhancement of the fluorescence of ZnP–CONH–Q results from the strong binding of $Y^{3+}$ to the quinone moiety, which causes a significant increase in the $\lambda$ value to retard the photoinduced electron transfer despite the larger driving force of electron transfer. Thus, the fluorescent property of a electron donor–acceptor dyad can be finely modulated by coordination of metal ions. This has lead to a rational design to develop fluorescence sensors.[66]

### Photocatalytic Oxygenation of Anthracenes and Olefins with Dioxygen Using 9-Mesityl-10-methylacridinium Ion

The long-lived electron-transfer state ($Acr^{\bullet}$–$Mes^{\bullet+}$), which has both the high oxidizing ability and the reducing ability (Fig. 5), has enabled us to utilize $Acr^+$–Mes as an efficient photocatalyst for radical coupling reactions between radical cations and radical anions, which can be produced by the electron-transfer oxidation and reduction of external electron donors and acceptors, respectively (vide infra).[67]

Visible light irradiation ($\lambda > 430$ nm) of the absorption band of $Acr^+$–Mes ($1.0 \times 10^{-3}$ M) in an $O_2$-saturated acetonitrile (MeCN) solution containing anthracene derivatives ($1.0 \times 10^{-2}$ M) results in formation of the oxygenation products, i.e., epidioxyanthracenes (Eq. 3).[67]

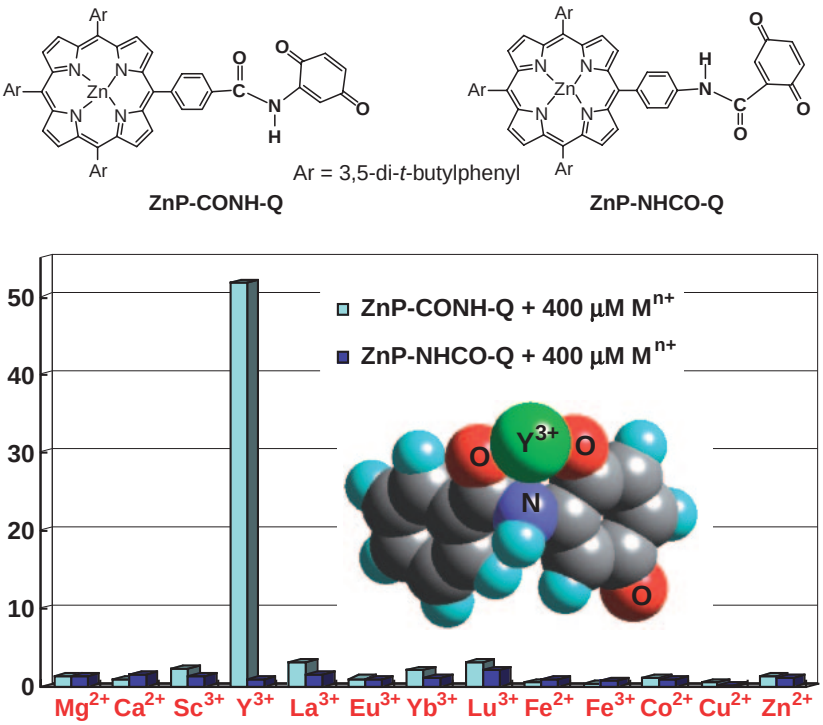


Fig. 7. Fluorescence responses ($I/I_0$ at 610 nm) of ZnP–CONH–Q and ZnP–NHCO–Q (3 μM) in the presence of 400 μM metal ions excited at 560 nm in reference to those in the absence of metal ion in deaerated PhCN; $CF_3OSO_3^-$ salt ($Ca^{2+}$, $Sc^{3+}$, $Y^{3+}$, $La^{3+}$, $Eu^{3+}$, $Yb^{3+}$, $Lu^{3+}$, and $Zn^{2+}$), $ClO_4^-$ salt ($Mg^{2+}$, $Fe^{2+}$, $Fe^{3+}$, $Co^{2+}$, and $Cu^{2+}$). Inset: The optimized structure of Ph–CONH–Q/$Y^{3+}$ complex is obtained by ADF calculation with II (large) basis set.

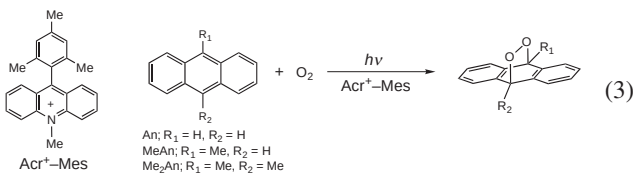


The photocatalytic oxygenation of $Me_2An$ with $O_2$ in a preparative scale (100 mg, $5.0 \times 10^{-4}$ mol) with $Acr^+$–Mes (8.2 mg, $2.0 \times 10^{-5}$ mol) resulted in isolation of dimethylepidioxyanthracene ($Me_2An$–$O_2$) in 80% yield.[67]

The addition of $Me_2An$ to MeCN solution of $Acr^+$–Mes and the laser photoexcitation result in formation of $Me_2An$ radical cation ($Me_2An^{\bullet+}$: $\lambda_{max} = 660$ nm)[68] with a concomitant decrease in the absorption band due to the $Mes^{\bullet+}$ moiety. The rate constant ($k_{et}$) of electron transfer from $Me_2An$ to the $Mes^{\bullet+}$ moiety of $Acr^{\bullet}$–$Mes^{\bullet+}$ is determined to be $1.4 \times 10^{10}$ $M^{-1}$ $s^{-1}$, which is close to be the diffusion-limited value as expected from the exergonic electron transfer. It is important to note that the absorption band due to the $Acr^{\bullet}$ moiety remains virtually the same in the absence of $O_2$. In the presence of $O_2$, the absorption band due to $Acr^{\bullet}$ moiety decays by electron transfer from the $Acr^{\bullet}$ moiety to $O_2$. The formation of $O_2^{\bullet-}$ was confirmed by the ESR spectrum measured at 233 K with the typical anisotropic $g$ values due to $O_2^{\bullet-}$ ($g_{\parallel} = 2.1050$ and $g_{\perp} = 2.0032$). The rate constant of electron transfer from the $Acr^{\bullet}$ moiety to $O_2$ ($k'_{et}$) was determined as $6.8 \times 10^8$ $M^{-1}$ $s^{-1}$. The absorbance at 660 nm due to $Me_2An^{\bullet+}$ in the presence of $O_2$ decays, obeying second-order kinetics, by the bimolecular reaction between $Me_2An^{\bullet+}$ and $O_2^{\bullet-}$. The second-order rate constant was determined as $1.7 \times 10^{10}$ $M^{-1}$ $s^{-1}$, which is close to the diffusion-limited value in MeCN. The quantum yields of the formation of anthracene radical cations in the presence of $O_2$ are significantly larger than those of the epidioxyanthracenes formation. This indicates that the back electron transfer from $O_2^{\bullet-}$ to anthracene radical cations to regenerate the reactant pair is also involved in the second-order decay of anthracene radical cations in addition to the radical coupling between anthracene radical cations and $O_2^{\bullet-}$ to afford the corresponding epidioxyanthracenes (Scheme 7). It was confirmed that An–$O_2$ is formed exclusively by the radical coupling between anthracene radical cation and $O_2^{\bullet-}$ ($k_c$) rather than the reaction of anthracene and $^1O_2$.[67]

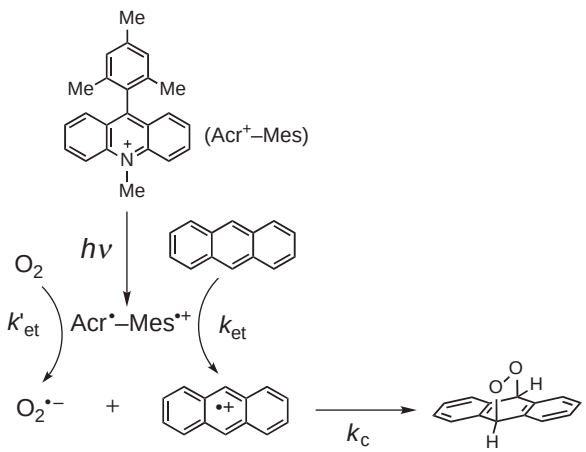


Scheme 7. Photocatalytic oxygenation of anthracene with $O_2$ using $Acr^+$–Mes.[67]

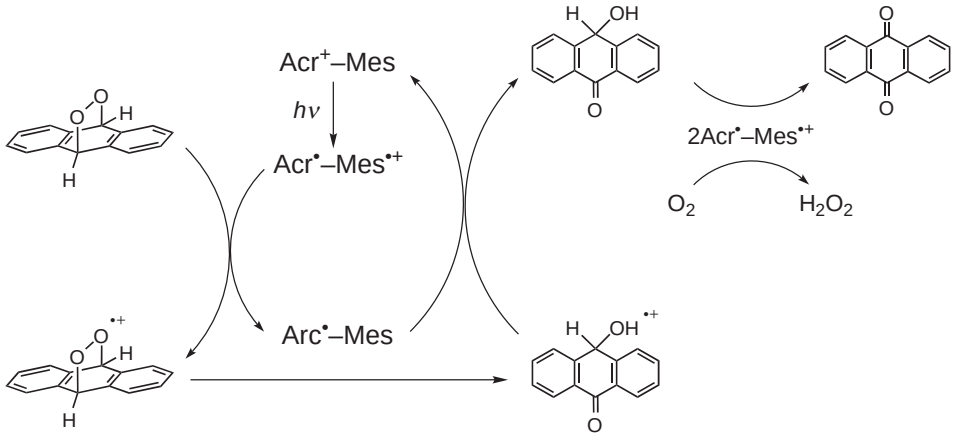


Scheme 8. Photocatalytic oxygenation of $AnO_2$ to anthraquinone with $Acr^+$–Mes.[67]

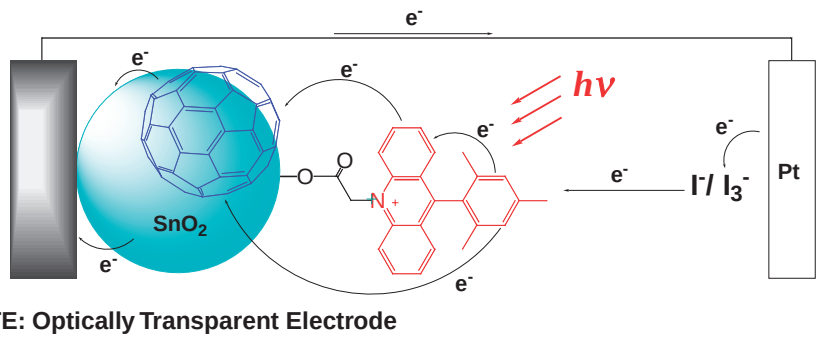


Scheme 9. The photovoltaic cell composed of fullerene nanoclusters and 9-mesityl-10-carboxymethylacridinium ion.[69]

In the case of anthracene, An–$O_2$ is converted to 10-hydroxyanthrone, which is further oxidized to yield the final six-electron oxidation product, i.e., anthraquinone, accompanied by generation of $H_2O_2$ with the further photoirradiation ($\lambda >$ 430 nm) of an $O_2$-saturated $CD_3CN$ solution of An–$O_2$ and $Acr^+$–Mes.[67] When the reaction is started from the isolated An–$O_2$, no photochemical reaction has occurred without $Acr^+$–Mes or no thermal reaction has taken place with $Acr^+$–Mes.[67] Under photoirradiation in the presence of $Acr^+$–Mes, electron transfer from An–$O_2$ to the $Mes^{\bullet+}$ moiety of $Acr^{\bullet}$–$Mes^{\bullet+}$ results in the O–O bond cleavage of An–$O_2^{\bullet+}$, followed by facile intramolecular hydrogen transfer to produce the 10-hydroxyanthrone radical cation as shown in Scheme 8.[67] The back electron transfer from the $Acr^{\bullet}$ moiety to 10-hydroxyanthrone radical cation affords 10-hydroxyanthrone, accompanied by regeneration of $Acr^+$–Mes. The electron-transfer oxidation of 10-hydroxyanthrone by the $Mes^{\bullet+}$ moiety of $Acr^{\bullet}$–$Mes^{\bullet+}$ results in the further two-electron oxidation to yield anthraquinone by releasing two protons, whereas the two-electron reduction of $O_2$ by the $Ac^{\bullet}$ moiety of $Acr^{\bullet}$–$Mes^{\bullet+}$ with two protons yields $H_2O_2$ (Scheme 8).

The radical coupling reaction between anthracene radical cation and $O_2^{\bullet-}$ to produce An–$O_2$ in Scheme 7 can be expanded to the dioxetane formation from olefins. Thus, the use of $Acr^+$–Mes as an electron-transfer photocatalyst in the presence of $O_2$ provides a convenient methodology to produce radical cations of electron donors of anthracenes and olefins as well as $O_2^{\bullet-}$, which can combine together to yield the oxygenated products selectively in a preparative scale.

## Photoelectrochemical Applications of Simple Donor–Acceptor Dyads

A simple molecular dyad ($Acr^+$–Mes) capable of fast charge separation but extremely slow charge recombination has now allowed us to develop a unique organic photovoltaic cell using the molecular dyad with an extremely long lifetime of the electron-transfer state as well as a high energy (2.37 eV). A carboxyl group was attached to the dyad to yield 9-mesityl-10-carboxymethylacridinium ion (Mes–$Acr^+$–COOH), which can be assembled on an optically transparent electrode (OTE) of nanostructured $SnO_2$ (OTE/$SnO_2$) to construct the organic photovoltaic cell composed of Mes–$Acr^+$–COOH and fullerene nanoclusters (Scheme 9).[69]

The synthesized dyad (Mes–$Acr^+$–COOH) was adsorbed by immersing OTE/$SnO_2$ electrode in an ethanol solution overnight to prepare OTE/$SnO_2$/Mes–$Acr^+$–COOH electrode.[69] In order to improve the light-harvesting efficiency, we deposited fullerene ($C_{60}$) clusters from $C_{60}$ suspension in acetonitrile/toluene (3/1) electrophoretically on the OTE/$SnO_2$/Mes–$Acr^+$–COOH electrode (denoted as OTE/$SnO_2$/Mes–$Acr^+$–COOH+$(C_{60})_n$). As reported previously, $C_{60}$ clusters act as good electron acceptors as well as light-harvesting molecules.[70] Photoelectrochemical measurements were performed using a standard two-electrode system consisting of a working electrode and a Pt wire gauze electrode in air-saturated acetonitrile containing 0.5 mol dm$^{-3}$ NaI and 0.01 mol dm$^{-3}$ $I_2$.[69] The IPCE (incident photon-to-photocurrent efficiency) values were calculated by normalizing the photocurrent values for

incident light energy and intensity and using Eq. 4,[69,70]

$$\text{IPCE}\ (\%) = 100 \times 1240 \times i_{sc}/(I_{inc} \times \lambda), \quad (4)$$

where $i_{sc}$ is the short circuit photocurrent (A/cm$^2$), $I_{inc}$ is the incident light intensity (W/cm$^2$), and $\lambda$ is the wavelength (nm). The maximum IPCE value of OTE/$SnO_2$/Acr$^+$–Mes–COOH (spectrum a in Fig. 8) is only 2% (445 nm), whereas the IPCE value of OTE/$SnO_2$/Acr$^+$–Mes–COOH+$(C_{60})_n$ (spectrum c in Fig. 8) reaches 15% (480 nm).[69] The IPCE value of OTE/$SnO_2$/Acr$^+$–Mes–COOH+$(C_{60})_n$ is much higher than the sum of the two individual IPCE values of the individual systems (OTE/$SnO_2$/Acr$^+$–Mes–COOH and OTE/$SnO_2$/$(C_{60})_n$; spectrum d in Fig. 8) in the visible region.[69]

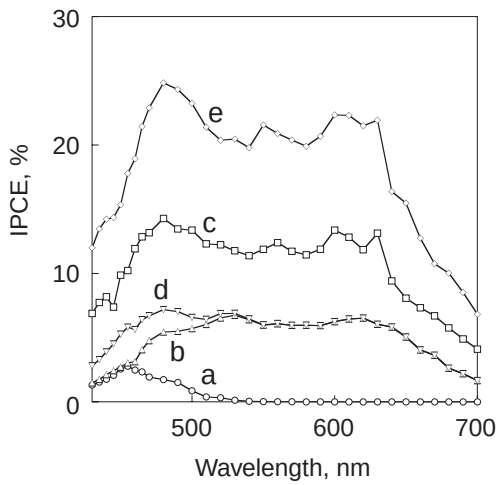


Fig. 8. Comparison of plots of IPCE vs wavelength of (a) OTE/$SnO_2$/Mes–Acr$^+$–COOH electrode ([$C_{60}$] = 0.62 mM), (b) OTE/$SnO_2$/$(C_{60})_n$ electrode ([$C_{60}$] = 0.62 mM), (c) OTE/$SnO_2$/Mes–Acr$^+$–COOH+$(C_{60})_n$ electrode ([$C_{60}$] = 0.62 mM), (d) the sum of the IPCE response of OTE/$SnO_2$/Mes–Acr$^+$–COOH and OTE/$SnO_2$/$(C_{60})_n$ electrodes ([$C_{60}$] = 0.62 mM), and (e) OTE/$SnO_2$/Mes–Acr$^+$–COOH+$(C_{60})_n$ electrode ([$C_{60}$] = 0.62 mM) with applied bias potential: 0.2 V vs SCE.

The charge separation in the OTE/$SnO_2$/Mes–Acr$^+$–COOH+$(C_{60})_n$ electrode can be further modulated by controlling the applied potential in a standard three-compartment cell with a working electrode along with a Pt wire gauze counter electrode and a saturated calomel reference electrode (SCE).[69] The maximum IPCE value is obtained as 25% at an applied potential of 0.2 V vs SCE (spectrum e in Fig. 8).[69] Such a high IPCE value indicates that photocurrent is initiated via electron-transfer between excited Mes–Acr$^+$–COOH and $C_{60}$ clusters, followed by the charge transport to the collective surface of OTE/$SnO_2$ electrode. The charge transport is significantly improved under the influence of an applied bias.

The mechanism of the photocurrent generation of OTE/$SnO_2$/Mes–Acr$^+$–COOH and OTE/$SnO_2$/Mes–Acr$^+$–COOH+$(C_{60})_n$ electrodes is summarized in Scheme 10.[69] The photocurrent generation is initiated by photoinduced electron transfer in Mes–Acr$^+$ dyad to produce Mes$^{\bullet+}$–Acr$^\bullet$. The resulting acridinyl radical (Acr$^\bullet$) (Acr$^+$/Acr$^\bullet$ = −0.3 V vs NHE) injects electrons into the conduction band of $SnO_2$ (0 V vs NHE),[70] whereas the oxidized mesityl moiety (Mes/Mes$^{\bullet+}$ = 2.0 V vs NHE) undergoes the electron-transfer reduction with the iodide ($I_3^-/I^-$ = 0.5 V vs NHE)[70] in the electrolyte solution. The long lifetime of the electron-transfer state (Mes$^{\bullet+}$–Acr$^\bullet$) ensures efficient electron transfer from Acr$^\bullet$ to $C_{60}$ ($C_{60}/C_{60}^{\bullet-}$ = −0.2 V vs NHE)[70] to produce $C_{60}^{\bullet-}$, which injects an electron into the conduction band of $SnO_2$. On the other hand, the oxidized mesityl moiety (Mes$^{\bullet+}$) undergoes the electron-transfer reduction with iodide ion in the electrolyte. Enhanced IPCE values of OTE/$SnO_2$/Mes–Acr$^+$–COOH+$(C_{60})_n$ (spectrum c in Fig. 8) relative to the sum of the two individual IPCE values of the individual systems (spectrum d in Fig. 8) may result from charge-transfer interaction between the mesityl (donor) moiety of Mes–Acr$^+$–COOH and $C_{60}$ clusters, which appears at the long wavelength region beyond 500 nm.[69] Thus, we have successfully constructed supramolecular photovoltaic cells using molecular nanocluster

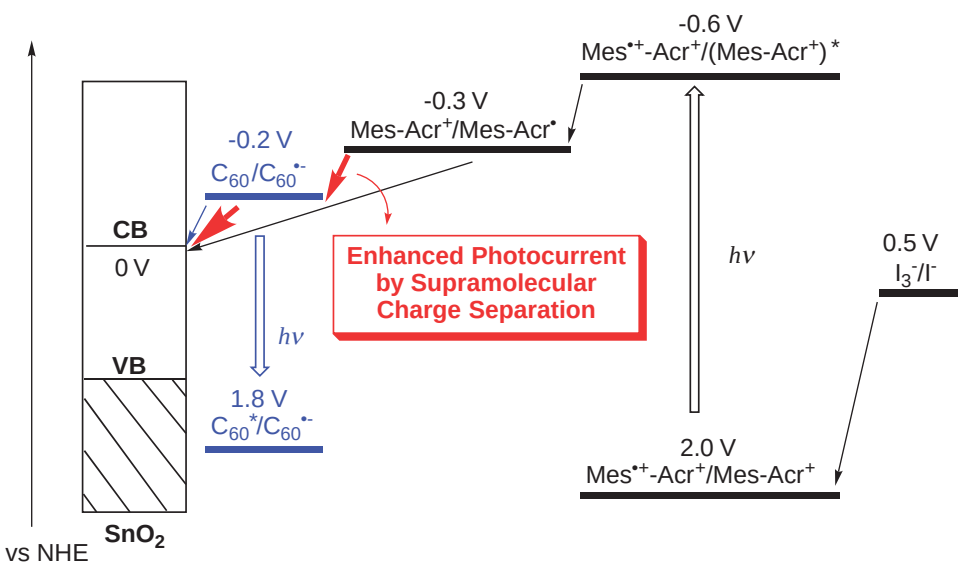


Scheme 10. Mechanism of the photocurrent generation in OTE/$SnO_2$/Mes–Acr$^+$–COOH+$(C_{60})_n$ electrode.

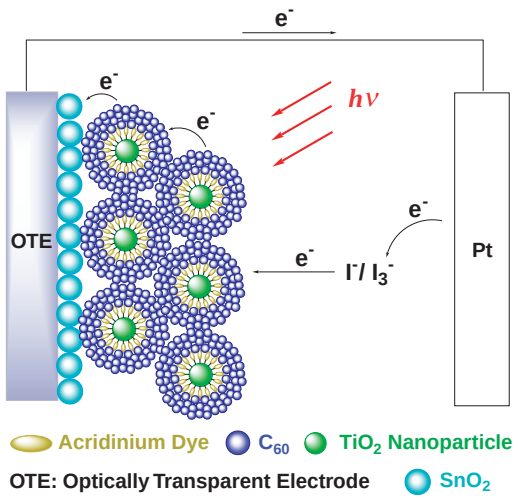


Scheme 11. Supramolecular photovoltaic cells based on composite molecular clusters of 9-mesityl-10-carboxymethylacridinium ion and fullerene, which is electrophoretically organized by $TiO_2$ nanoparticles.[71]

assemblies of fullerene and a simple molecular dyad (Mes–$Acr^+$) with an extremely long lifetime and a high energy of the electron-transfer state.

$TiO_2$ nanoparticles have been utilized for three-dimensional control in organization of the donor–acceptor composite molecules to improve the photoelectrochemical properties.[71] $TiO_2$ nanoparticles modified with composite nanoclusters of Mes–$Acr^+$–COOH and $C_{60}$ in acetonitrile/toluene (3:1, v/v) were deposited as thin films on nanostructured $SnO_2$ electrode using an electrophoretic technique (Scheme 11).[71] The IPCE value of 37% has been achieved at an applied bias potential of 0.2 V vs SCE in the Mes–$Acr^+$–COOH/$C_{60}$ composite system using $TiO_2$ nanoparticles.[71]

## Catalytic Mechanism of Four-Electron Reduction of Dioxygen to Water

The highly exergonic four-electron reduction of $O_2$ to water, which is the reverse process of photosynthesis, plays a vital role to maintain the life of an aerobic organism by the respiration.[18–20] Cytochrome *c* oxidases (C*c*Os) are responsible for catalyzing the reduction of $O_2$ to water by the soluble electron carrier, cytochrome *c*.[18–20] The four-electron reduction of $O_2$ is not only of great biological interest,[18–20] but also of technological significance such as fuel cells.[72] Thus, a number of synthetic analogs of the active center of C*c*Os have so far been synthesized to mimic the coordination environment of the Fe/Cu core as well as the catalytic function of the four-electron reduction of $O_2$.[73] The most important question of how the C*c*O enzyme catalyzes the four-electron reduction of $O_2$ to water without releasing the two-electron reduced species ($H_2O_2$) has been clarified by studying the catalytic four-electron reduction of $O_2$ vs two-electron reduction of $O_2$ using a one-electron reductant in a homogeneous solution.

It has been reported that the four-electron reduction of $O_2$ by ferrocene derivatives, which are one-electron reductants, are efficiently catalyzed by cofacial dicobalt porphyrins in the presence of perchloric acid ($HClO_4$) in PhCN, as shown in Scheme 12. The cofacial dicobalt porphyrins are chosen as catalysts for the four-electron reduction of $O_2$, because the bimetallic system is indispensable for the four-electron reduction of $O_2$ in the case of cobalt porphyrins, thus allowing for the difference from the single metal system to be clarified.

Based on the detailed kinetic comparison of the catalytic reactivities of cofacial dicobalt porphyrins and a single cobalt porphyrin, together with the detection of the reactive intermediates by ESR, the catalytic mechanism of four-electron reduction of $O_2$ by ferrocene derivatives is summarized as shown in Scheme 13. The initial two-electron reduction of the $Co(III)_2$ complex by ferrocene derivatives gives the $Co(II)_2$ complex, which reacts with $O_2$ to produce the $\mu$-peroxo Co(III)–$O_2$–Co(III) complex. The heterolytic O–O-bond cleavage of the Co(III)–$O_2$–Co(III) complex affords the high valent Co(IV)oxo porphyrin $\pi$-radical cation, which is reduced by ferrocene derivatives in the presence of proton to yield $H_2O$ (Scheme 13).[75] The critical point to distinguish between the two-electron and four-electron reduction pathways is formation of the $\mu$-peroxo Co(III)–$O_2$–Co(III) complex, which requires an appropriate Co–Co distance in the cofacial dicobalt complex. The Co–Co distance in $Co_2$(DPX) is best suited for formation of the $\mu$-peroxo Co(III)–$O_2$–Co(III) complex, resulting in the catalytic four-electron reduction of $O_2$.[74] In the case of monomeric cobalt porphyrins such as $Co(TPP)^+$ (TPP = tetraphenylporphyrin) and Co(OEP) (OEP = octaethylporphyrin), there is no way to form the $\mu$-peroxo Co(III)–$O_2$–Co(III) complex.[76] In such a case, the protonation of the Co(III)$O_2$H complex yields $H_2O_2$, resulting in only two-electron reduction of $O_2$.

The kinetic study has indicated that the proton-coupled electron transfer from Co(III)Co(II)$(DPX)^+$, which is produced in the initial electron transfer from $Fe(C_5H_5)_2$ and $Fe(C_5H_4Me)_2$ to $Co(III)_2(DPX)^{2+}$, to $O_2$ is the turnover-determining step in the catalytic four-electron reduction of $O_2$ in Scheme 12.[74] When $Fe(C_5H_5)_2$ is replaced by a much stronger reductant than $Fe(C_5H_5)_2$ or $Fe(C_5H_4Me)_2$, that is $Fe(C_5Me_5)_2$, the turnover-determining step changes from the proton-coupled electron transfer from Co(III)Co(II)$(DPX)^+$ to $O_2$ in the case of

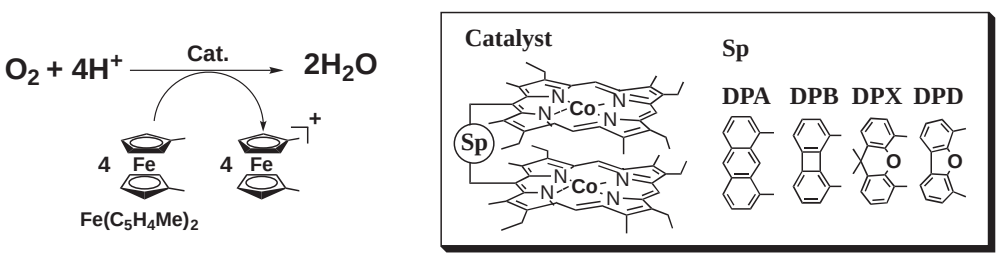


Scheme 12. Catalytic four-electron reduction of $O_2$ by a ferrocene derivative with cofacial dicobalt porphyrins.[74]

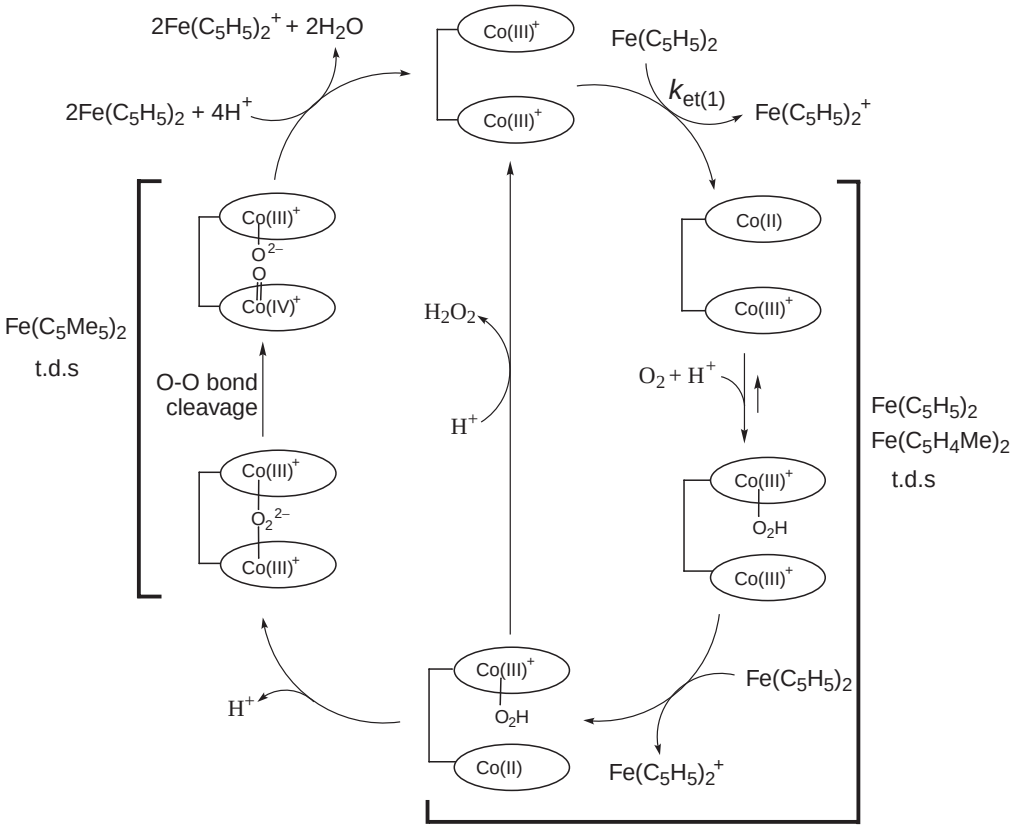


Scheme 13. The catalytic mechanism of four-electron reduction of $O_2$ by ferrocene with a cofacial cobalt porphyrin.[74]

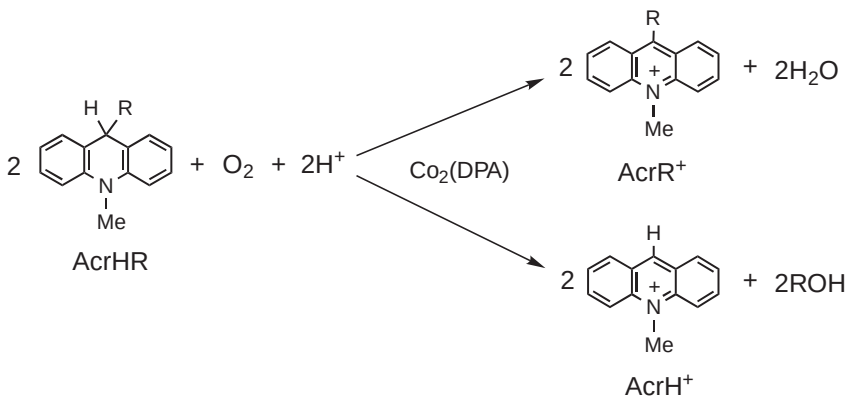


Scheme 14. Catalytic dehydration vs oxygenation of the R group of AcrHR with $Co_2$(DPA).[77]

$Fe(C_5H_5)_2$ or $Fe(C_5H_4Me)_2$ to the O–O bond cleavage step of the Co(III)–$O_2$–Co(III) complex in Scheme 13.[74] The O–O bond cleavage rate has been determined as $320\ s^{-1}$.[74]

The $Co_2$(DPA)-catalyzed reduction of $O_2$ also occurs efficiently by an NADH analogue (a two-electron reductant), 9-alkyl-10-methyl-9,10-dihydroacridine (AcrHR: R = Me, Et, and $CH_2COOEt$), to yield 9-alkyl-10-methylacridinium ion ($AcrR^+$) and $H_2O$ (Scheme 14).[77] In the case of R = $Bu^t$ and $CMe_2COOMe$, however, the catalytic reduction of $O_2$ by AcrHR results in oxygenation of the alkyl group of AcrHR rather than the dehydrogenation to yield 10-methylacridinium ion ($AcrH^+$) and ROH (Scheme 14).[77]

In the case of $AcrH_2$, the initial slow electron transfer from $AcrH_2$ to the $Co(III)_2$ complex is followed by the C(9)–H cleavage in competition with the back electron transfer from the Co(III)Co(II) complex to $AcrH_2^{\bullet+}$ to produce $AcrH^{\bullet}$.[77] Since the catalytic rate-determining step is deprotonation of $AcrH_2^{\bullet+}$, the Co(III)Co(II) complex reacts rapidly with $O_2$ and $H^+$ to give the Co(III)Co(III)$O_2$H complex, followed by electron transfer from $AcrH^{\bullet}$ to the Co(III)Co(III)$OH_2$ complex to produce $AcrH^+$ and the Co(II)Co(III)$OH_2$ complex. After deprotonation, the $\mu$-peroxo Co(III)–$O_2$–Co(III) complex is formed as in the case of the catalytic four-electron reduction of $O_2$ by ferrocene derivatives.[74] The heterolytic O–O-bond cleavage of the Co(III)–$O_2$–Co(III) complex affords the high valent Co(IV)oxo porphyrin $\pi$-radical cation, which is readily reduced by $AcrH_2$ in the presence of a proton to yield $H_2O$, accompanied by formation of $AcrH^+$.

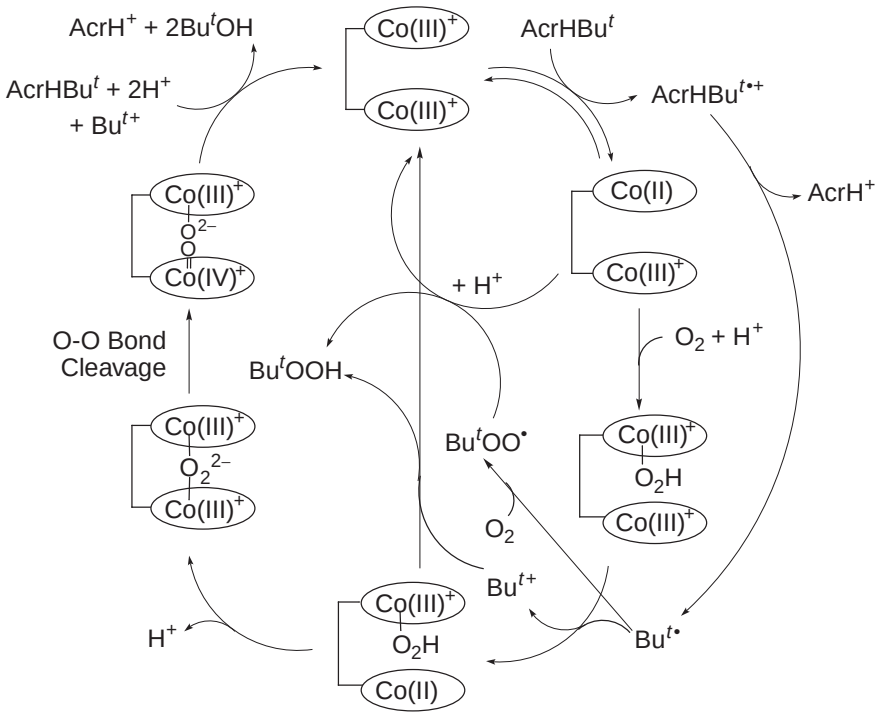


Scheme 15. Mechanism of the catalytic oxygenation of the R group of AcrHR by $O_2$ with a cofacial cobalt porphyrin.[77]

In the case of AcrHBu$^t$, the mechanism of the catalytic four-electron reduction of $O_2$, accompanied by the oxygenation of Bu$^t$, is modified as shown in Scheme 15. The initial electron transfer from AcrHBu$^t$ to the Co(III)$_2$ complex results in the homolytic C(9)–C bond cleavage to produce Bu$^{t\bullet}$ and AcrH$^+$.[78] Since the homolytic C(9)–C bond cleavage is also the catalytic rate-determining step, the Co(III)Co(III)$O_2$H complex is formed by the reaction of $O_2$ and $H^+$, followed by electron transfer from Bu$^{t\bullet}$ ($E_{ox} = 0.09$ V vs SCE)[79] to the Co(III)Co(III)$O_2$H complex to produce Bu$^{t+}$ and the Co(II)Co(III)$O_2$H complex. The subsequent step may be the same as the case of the four-electron reduction of $O_2$ by AcrH$_2$. The high valent Co(IV)oxo porphyrin $\pi$-radical cation is formed by the heterolytic O–O-bond cleavage of the Co(III)–$O_2$–Co(III) complex, being reduced by AcrHBu$^t$ in the presence of proton to yield Bu$^t$OH, accompanied by formation of AcrH$^+$ (Scheme 15). However, Bu$^{t\bullet}$ produced in the initial electron transfer from AcrHBu$^t$ to the Co(III)$_2$ complex is readily trapped by $O_2$ to give the peroxyl radical Bu$^t$OO$^\bullet$.[80] Such alkylperoxyl radicals (ROO$^\bullet$) are regarded as rather strong one-electron oxidants judging from the highly positive one-electron reduction potentials.[81] Thus, the initial electron transfer from AcrHBu$^t$ to the Co(III)$_2$ complex may also be followed by the subsequent electron transfer from the Co(III)Co(II) complex to Bu$^t$OO$^\bullet$ to produce Bu$^t$OOH after protonation, accompanied by regeneration of the Co(III)$_2$ complex (Scheme 15).

In conclusion, the four-electron reduction of $O_2$ by AcrHR catalyzed by cofacial dicobalt porphyrins occurs efficiently via the electron transfer from AcrHR to cofacial dicobalt porphyrins, followed by the C(9)–H and C(9)–C bond cleavage of AcrHR$^{\bullet+}$ depending on the type of R, leading to the dehydration and oxygenation of AcrHR, respectively. In each case, the formation of the $\mu$-peroxo Co(III)–$O_2$–Co(III) complex plays a crucial role for the four-electron reduction of $O_2$ by AcrHR.

## Conclusion

As demonstrated in this review, bioinspired approaches are important in order to design electron-transfer systems including artificial photosynthesis and respiration. The strategies to construct artificial electron-transfer systems are not necessarily the same as those employed in natural systems, although the basic principle to control the electron-transfer processes is the same in light of the Marcus theory of electron transfer. In artificial photosynthesis, simple molecular dyads have been shown to be capable of fast charge separation but extremely slow charge recombination with minimized energy loss, whereas a significant amount of energy loss is required for the long-range charge separation in the multi-step electron-transfer processes in natural photosynthetic reaction centers. Such readily synthesized donor–acceptor dyads can be successfully applied to construct efficient photocatalytic systems as well as organic solar cells. Electron-transfer processes of donor–acceptor dyads containing quinones can be finely modulated by coordination of metal ions. The control of electron-transfer processes by coordination of metal ions to the dyads has led us to develop a unique fluorescence sensor for $Y^{3+}$ ion. A strong binding of one-electron reduced species with metal ion plays an important role in the electron-transfer reduction of $O_2$. In particular, the formation of the $\mu$-peroxo Co(III)–$O_2$–Co(III) complex is essential for the catalytic four-electron reduction of $O_2$. The scope and the applications of bioinspired electron-transfer systems are expected to expand much further in the future.

The author greatfully acknowledges the contributions of his collaborators mentioned in the references. The author thanks the Ministry of Education, Culture, Sports, Science and Technology, Japan, for the continuous support.

## References


1 U. Ermler, G. Fritzsch, S. K. Buchanan, H. Michel, *Structure* **1994**, *2*, 925.

2 J. Deisenhofer, H. Michel, *Science* **1989**, *245*, 1463.

3 A. J. Hoff, J. Deisenhofer, *Phys. Rep.* **1997**, *287*, 2.

4 L. C. Williams, A. K. W. Taguchi, *Anoxygenic Photosynthetic Bacteria*, ed. by R. E. Blankenship, M. T. Madigan, C. E. Bauer, Kluwer, Dordrecht, **1995**, p. 1029.

5 C. Kirmaier, D. Holten, W. W. Parson, *Biochim. Biophys. Acta* **1985**, *810*, 49.

6 D. J. Lockhart, C. Kirmaier, D. Holten, S. G. Boxer, *J. Phys. Chem.* **1990**, *94*, 6987.

7 S. G. Boxer, *Annu. Rev. Biophys. Biophys. Chem.* **1990**, *19*, 267.

8 *The Photosynthetic Reaction Center*, ed. by J. Deisenhofer, J. R. Norris, Academic Press, San Diego, **1993**.

9 a) D. Gust, T. A. Moore, A. L. Moore, *Acc. Chem. Res.* **1993**, *26*, 198. b) D. Gust, T. A. Moore, A. L. Moore, *Acc. Chem. Res.* **2001**, *34*, 40.

10 a) M. R. Wasielewski, *Chem. Rev.* **1992**, *92*, 435. b) M. N. Paddon-Row, *Acc. Chem. Res.* **1994**, *17*, 18. c) K. D. Jordan, M. N. Paddon-Row, *Chem. Rev.* **1992**, *92*, 395. d) J. W. Verhoeven, *Adv. Chem. Phys.* **1999**, *106*, 603.

11 M.-J. Blanco, M. C. Jiménez, J.-C. Chambron, V. Heitz, M. Linke, J.-P. Sauvage, *Chem. Soc. Rev.* **1999**, *28*, 293.

12 A. Osuka, N. Mataga, T. Okada, *Pure Appl. Chem.* **1997**, *69*, 797.

13 S. Fukuzumi, H. Imahori, *Electron Transfer in Chemistry*, ed. by V. Balzani, Wiley-VCH, Weinheim, **2001**, Vol. 2, pp. 927–975.

14 S. Fukuzumi, D. M. Guldi, in *Electron Transfer in Chemistry*, ed. by V. Balzani, Wiley-VCH, Weinheim, **2001**, Vol. 2, pp 270–337.

15 S. Fukuzumi, H. Imahori, *Photochemistry of Organic Molecules in Isotropic and Anisotropic Media*, ed. by V. Ramamurthy, K. S. Schanze, Marcel Dekker, New York, **2003**, pp. 227–273.

16 D. M. Guldi, S. Fukuzumi, *Fullerenes: From Synthesis to Optoelectronic Properties*, ed. by D. M. Guldi, N. Martin, Kluwer, Dordrecht, **2003**, pp. 237–265.

17 S. Fukuzumi, *Org. Biomol. Chem.* **2003**, *1*, 609.

18 a) G. T. Babcock, M. Wikström, *Nature* **1992**, *356*, 301. b) G. T. Babcock, *Proc. Natl. Acad. Sci. U.S.A.* **1999**, *96*, 12971.

19 a) M. Wikström, K. Krab, M. Saraste, *Cytochrome Oxidase: A Synthesis*, Academic Press, New York, **1981**. b) S. Ferguson-Miller, G. T. Babcock, *Chem. Rev.* **1996**, *96*, 2889.

20 a) M. M. Pereira, M. Santana, M. Teixeira, *Biochim. Biophys. Acta* **2001**, *1505*, 185. b) D. Zaslavsky, R. B. Gennis, *Biochim. Biophys. Acta* **2000**, *1458*, 164.

21 a) R. A. Marcus, *Angew. Chem., Int. Ed. Engl.* **1993**, *32*, 1111. b) R. A. Marcus, N. Sutin, *Biochim. Biophys. Acta* **1985**, *811*, 265.

22 a) J. R. Miller, L. T. Calcaterra, G. L. Closs, *J. Am. Chem. Soc.* **1984**, *106*, 3047. b) G. L. Closs, J. R. Miller, *Science* **1988**, *240*, 440. c) I. R. Gould, S. Farid, *Acc. Chem. Res.* **1996**, *29*, 522. d) G. McLendon, *Acc. Chem. Res.* **1988**, *21*, 160. e) J. R. Winkler, H. B. Gray, *Chem. Rev.* **1992**, *92*, 369. f) G. McLendon, R. Hake, *Chem. Rev.* **1992**, *92*, 481.

23 S. Fukuzumi, *The Porphyrin Handbook*, ed. by K. M. Kadish, K. Smith, R. Guilard, Academic Press, San Diego, **2000**, Vol. 8, pp. 115–151.

24 S. Fukuzumi, K. Ohkubo, H. Imahori, D. M. Guldi, *Chem. Eur. J.* **2003**, *9*, 1585.

25 H. Imahori, K. Tamaki, D. M. Guldi, C. Luo, M. Fujitsuka, O. Ito, Y. Sakata, S. Fukuzumi, *J. Am. Chem. Soc.* **2001**, *123*, 2607.

26 H. Imahori, D. M. Guldi, K. Tamaki, Y. Yoshida, C. Luo, Y. Sakata, S. Fukuzumi, *J. Am. Chem. Soc.* **2001**, *123*, 6617.

27 H. Imahori, M. E. El-Khouly, M. Fujitsuka, O. Ito, Y. Sakata, S. Fukuzumi, *J. Phys. Chem. A* **2001**, *105*, 325.

28 H. Imahori, N. V. Tkachenko, V. Vehmanen, K. Tamaki, H. Lemmetyinen, Y. Sakata, S. Fukuzumi, *J. Phys. Chem. A* **2001**, *105*, 1750.

29 S. Fukuzumi, H. Imahori, H. Yamada, M. E. El-Khouly, M. Fujitsuka, O. Ito, D. M. Guldi, *J. Am. Chem. Soc.* **2001**, *123*, 2571.

30 H. Imahori, K. Tamaki, Y. Araki, Y. Sekiguchi, O. Ito, Y. Sakata, S. Fukuzumi, *J. Am. Chem. Soc.* **2002**, *124*, 5165.

31 A. Helms, D. Heiler, G. McLendon, *J. Am. Chem. Soc.* **1992**, *114*, 6227.

32 H. Imahori, Y. Sekiguchi, Y. Kashiwagi, T. Sato, Y. Araki, O. Ito, H. Yamada, S. Fukuzumi, *Chem. Eur. J.* **2004**, *10*, 3184.

33 K. N. Ferreira, T. M. Iverson, K. Maghlaoui, J. Barber, S. Iwata, *Science* **2004**, *303*, 1831.

34 Y. Kashiwagi, K. Ohkubo, J. A. McDonald, I. M. Blake, M. J. Crossley, Y. Araki, O. Ito, H. Imahori, S. Fukuzumi, *Org. Lett.* **2003**, *5*, 2719.

35 S. Fukuzumi, K. Ohkubo, W. E. Z. Ou, J. Shao, K. M. Kadish, J. A. Hutchison, K. P. Ghiggino, P. J. Sintic, M. J. Crossley, *J. Am. Chem. Soc.* **2003**, *125*, 14984.

36 K. Ohkubo, H. Kotani, J. Shao, Z. Ou, K. M. Kadish, G. Li, R. K. Pandey, M. Fujitsuka, O. Ito, H. Imahori, S. Fukuzumi, *Angew. Chem., Int. Ed.* **2004**, *43*, 853.

37 S. Fukuzumi, K. Ohkubo, H. Imahori, J. Shao, Z. Ou, G. Zheng, Y. Chen, R. K. Pandey, M. Fujitsuka, O. Ito, K. M. Kadish, *J. Am. Chem. Soc.* **2001**, *123*, 10676.

38 K. Ohkubo, H. Imahori, J. Shao, Z. Ou, K. M. Kadish, Y. Chen, G. Zheng, R. K. Pandey, M. Fujitsuka, O. Ito, S. Fukuzumi, *J. Phys. Chem. A* **2002**, *106*, 10991.

39 N. V. Tkachenko, H. Lemmetyinen, J. Sonoda, K. Ohkubo, T. Sato, H. Imahori, S. Fukuzumi, *J. Phys. Chem. A* **2003**, *107*, 8834.

40 T. J. Kesti, N. V. Tkachenko, V. Vehmanen, H. Yamada, H. Imahori, S. Fukuzumi, H. Lemmetyinen, *J. Am. Chem. Soc.* **2002**, *124*, 8067.

41 a) D. G. Johnson, M. P. Niemczyk, D. W. Minsek, G. P. Wiederrecht, W. A. Svec, G. L. Gaines, III, M. R. Wasielewski, *J. Am. Chem. Soc.* **1993**, *115*, 5692. b) Y. Sakata, H. Tsue, M. P. O'Neil, G. P. Wiederrecht, M. R. Wasielewski, *J. Am. Chem. Soc.* **1994**, *116*, 6904. c) H. Tsue, H. Imahori, T. Kaneda, Y. Tanaka, T. Okada, K. Tamaki, Y. Sakata, *J. Am. Chem. Soc.* **2000**, *122*, 2279. d) Y. K. Kang, I. V. Rubtsov, P. M. Iovine, J. Chen, M. J. Therien, *J. Am. Chem. Soc.* **2002**, *124*, 8275.

42 a) T. Asahi, M. Ohkohchi, R. Matsusaka, N. Mataga, R. P. Zhang, A. Osuka, K. Maruyama, *J. Am. Chem. Soc.* **1993**, *113*, 5665. b) L. R. Khundkar, J. W. Perry, J. E. Hanson, P. B. Dervan, *J. Am. Chem. Soc.* **1994**, *116*, 9700. c) J. L. Sessler, B. Wang, A. Harriman, *J. Am. Chem. Soc.* **1993**, *115*, 10418.

43 In liquid crystals, the CR rates were attenuated into the submicrosecond time scale; see: a) A. Berman, E. S. Izraeli, H. Levanon, B. Wang, J. L. Sessler, *J. Am. Chem. Soc.* **1995**, *117*, 8252. b) A. Berg, Z. Shuali, H. Levanon, A. Wiehe, H. Kurreck, *J. Phys. Chem. A* **2001**, *105*, 10060.

44 H. Imahori, H. Yamada, D. M. Guldi, Y. Endo, A. Shimomura, S. Kundu, K. Yamada, T. Okada, Y. Sakata, S. Fukuzumi, *Angew. Chem., Int. Ed.* **2002**, *41*, 2344.

45 K. Okamoto, S. Fukuzumi, *J. Phys. Chem. B* **2005**, *109*, 7713.

46 S. Fukuzumi, K. Ohkubo, T. Suenobu, K. Kato, M. Fujitsuka, O. Ito, *J. Am. Chem. Soc.* **2001**, *123*, 8459.

47 K. Kikuchi, C. Sato, M. Watabe, H. Ikeda, Y. Takahashi, T. Miyashi, *J. Am. Chem. Soc.* **1993**, *115*, 5180.

48 K. Ohkubo, K. Suga, K. Morikawa, S. Fukuzumi, *J. Am. Chem. Soc.* **2003**, *125*, 12850.

49 S. Fukuzumi, H. Kotani, K. Ohkubo, S. Ogo, N. V. Tkachenko, H. Lemmetyinen, *J. Am. Chem. Soc.* **2004**, *126*, 1600.

50 A. Harriman, *Angew. Chem., Int. Ed.* **2004**, *43*, 4985.

51 A. C. Benniston, A. Harriman, P. Li, J. P. Rostron, J. W. Verhoeven, *Chem. Commun.* **2005**, 2701.

52 X. Guo, Z. Gan, H. Luo, Y. Araki, D. Zhang, D. Zhu, O. Ito, *J. Phys. Chem. A* **2003**, *107*, 9747.

53 K. Okamoto, Y. Mori, H. Yamada, H. Imahori, S. Fukuzumi, *Chem. Eur. J.* **2004**, *10*, 474.

54 H. Kotani, K. Ohkubo, S. Fukuzumi, *Chem. Commun.* **2005**, 4520.

55 T. Shida, *Electronic Absorption Spectra of Radical Ions*, Elsevier, Amsterdam, **1988**.

56 O. Morawski, J. Prochorow, *Chem. Phys. Lett.* **1995**, *242*, 253.

57 a) S. Fukuzumi, *Electron Transfer in Chemistry*, ed. by V. Balzani, Wiley-VCH, Weinheim, **2001**, Vol. 4, pp. 3–67. b) S. Fukuzumi, S. Itoh, *Advances in Photochemistry*, ed. by D. C. Neckers, D. H. Volman, G. von Bünau, Wiley, New York, **1998**, Vol. 25, pp. 107–172. c) S. Fukuzumi, *Bull. Chem. Soc. Jpn.* **1997**, *70*, 1.

58 a) S. Fukuzumi, S. Koumitsu, K. Hironaka, T. Tanaka, *J. Am. Chem. Soc.* **1987**, *109*, 305. b) S. Fukuzumi, N. Nishizawa, T. Tanaka, *J. Chem. Soc., Perkin Trans. 2* **1985**, 371.

59 a) S. Fukuzumi, T. Okamoto, J. Otera, *J. Am. Chem. Soc.* **1994**, *116*, 5503. b) S. Fukuzumi, N. Satoh, T. Okamoto, K. Yasui, T. Suenobu, Y. Seko, M. Fujitsuka, O. Ito, *J. Am. Chem. Soc.* **2001**, *123*, 7756. c) S. Fukuzumi, H. Mori, H. Imahori, T. Suenobu, Y. Araki, O. Ito, K. M. Kadish, *J. Am. Chem. Soc.* **2001**, *123*, 12458. d) S. Fukuzumi, Y. Fujii, T. Suenobu, *J. Am. Chem. Soc.* **2001**, *123*, 10191.

60 a) S. Fukuzumi, K. Ohkubo, T. Okamoto, *J. Am. Chem. Soc.* **2002**, *124*, 14147. b) S. Fukuzumi, O. Inada, N. Satoh, T. Suenobu, H. Imahori, *J. Am. Chem. Soc.* **2002**, *124*, 9181. c) S. Fukuzumi, J. Yuasa, T. Suenobu, *J. Am. Chem. Soc.* **2002**, *124*, 12566.

61 a) S. Fukuzumi, K. Okamoto, H. Imahori, *Angew. Chem., Int. Ed.* **2002**, *41*, 620. b) S. Fukuzumi, K. Okamoto, Y. Yoshida, H. Imahori, Y. Araki, O. Ito, *J. Am. Chem. Soc.* **2003**, *125*, 1007. c) K. Okamoto, H. Imahori, S. Fukuzumi, *J. Am. Chem. Soc.* **2003**, *125*, 7014.

62 a) S. Fukuzumi, K. Ohkubo, *Chem. Eur. J.* **2000**, *6*, 4532. b) S. Fukuzumi, K. Ohkubo, *J. Am. Chem. Soc.* **2002**, *124*, 10270. c) K. Ohkubo, S. C. Menon, A. Orita, J. Otera, S. Fukuzumi, *J. Org. Chem.* **2003**, *68*, 4720.

63 K. Okamoto, Y. Mori, H. Yamada, H. Imahori, S. Fukuzumi, *Chem. Eur. J.* **2004**, *10*, 474.

64 K. Okamoto, Y. Araki, O. Ito, S. Fukuzumi, *J. Am. Chem. Soc.* **2004**, *126*, 56.

65 K. Okamoto, S. Fukuzumi, *J. Am. Chem. Soc.* **2004**, *126*, 13922.

66 For rational design principle for modulating fluorescence properties of fluorescein-based probes by photoinduced electron transfer, see: T. Miura, Y. Urano, K. Tanaka, T. Nagano, K. Ohkubo, S. Fukuzumi, *J. Am. Chem. Soc.* **2003**, *125*, 8666.

67 H. Kotani, K. Ohkubo, S. Fukuzumi, *J. Am. Chem. Soc.* **2004**, *126*, 15999.

68 S. Fukuzumi, I. Nakanishi, K. Tanaka, *J. Phys. Chem. A* **1999**, *103*, 11212.

69 T. Hasobe, S. Hattori, H. Kotani, K. Ohkubo, K. Hosomizu, H. Imahori, P. V. Kamat, S. Fukuzumi, *Org. Lett.* **2004**, *6*, 3103.

70 a) T. Hasobe, H. Imahori, P. V. Kamat, S. Fukuzumi, *J. Am. Chem. Soc.* **2003**, *125*, 14962. b) T. Hasobe, H. Imahori, P. V. Kamat, T. K. Ahn, D. Kim, T. Hanada, T. Hirakawa, S. Fukuzumi, *J. Am. Chem. Soc.* **2005**, *127*, 1217. c) T. Hasobe, P. V. Kamat, V. Troiani, N. Solladié, T. K. Ahn, S. K. Kim, D. Kim, A. Kongkanand, S. Kuwabata, S. Fukuzumi, *J. Phys. Chem. B* **2005**, *109*, 19.

71 T. Hasobe, S. Hattori, P. V. Kamat, Y. Wada, S. Fukuzumi, *J. Mater. Chem.* **2005**, *15*, 372.

72 a) F. C. Anson, C. N. Shi, B. Steiger, *Acc. Chem. Res.* **1997**, *30*, 437. b) R. P. Kingsborough, T. M. Swager, *Adv. Mater.* **1998**, *10*, 1100.

73 a) J. P. Collman, R. Boulatov, C. J. Sunderland, *The Porphyrin Handbook*, ed. by K. M. Kadish, K. M. Smith, R. Guilard, Elsevier Science, U.S.A., **2003**, Vol. 11, pp. 1–49. b) J. P. Collman, L. Fu, P. C. Herrmann, X. M. Zhang, *Science* **1997**, *275*, 949.

74 S. Fukuzumi, K. Okamoto, C. P. Gros, R. Guilard, *J. Am. Chem. Soc.* **2004**, *126*, 10441.

75 Formation of high-valent cobalt-oxo complex has been suggested; see: W. Nam, I. Kim, Y. Kim, C. Kim, *Chem. Commun.* **2001**, 1296.

76 S. Fukuzumi, S. Mochizuki, T. Tanaka, *Inorg. Chem.* **1989**, *28*, 2459.

77 S. Fukuzumi, K. Okamoto, Y. Tokuda, C. P. Gros, R. Guilard, *J. Am. Chem. Soc.* **2004**, *126*, 17059.

78 a) S. Fukuzumi, Y. Tokuda, T. Kitano, T. Okamoto, J. Otera, *J. Am. Chem. Soc.* **1993**, *115*, 8960. b) S. Fukuzumi, K. Ohkubo, Y. Tokuda, T. Suenobu, *J. Am. Chem. Soc.* **2000**, *122*, 4286.

79 D. D. M. Wayner, D. J. McPhee, D. Griller, *J. Am. Chem. Soc.* **1988**, *110*, 132.

80 N. Takada, S. Itoh, S. Fukuzumi, *Chem. Lett.* **1996**, 1103.

81 S. Fukuzumi, K. Shimoosako, T. Suenobu, Y. Watanabe, *J. Am. Chem. Soc.* **2003**, *125*, 9074.

Shunichi Fukuzumi was born in Nagoya in 1950. He earned a bachelor's degree and Ph.D. degree in applied chemistry at Tokyo Institute of Technology in 1973 and 1978, respectively. After working as a postdoctoral fellow (1978–1981) at Indiana University in U. S. A., he joined the Department of Applied Chemistry, Osaka University, as an Assistant Professor in 1981 and was promoted to a Full Professor in 1994. His research interests are electron-transfer chemistry in all fields of chemistry. He has been the director of a CREST (Core Research for Evolutional Science and Technology) project of Japan Science and Technology Agency since 1999, which is now extended as a SORST (Solution Oriented Research for Science and Technology) project.